Università degli Studi di Salerno

Facoltà di Scienze Matematiche Fisiche e Naturali
Dipartimento di Matematica e Informatica

Dottorato di Ricerca in Matematica
X Ciclo – Nuova Serie

TESI DI DOTTORATO

Simulation and optimization of crowd dynamics using a multiscale model.

CANDIDATO: **LUIGI SORRENTINO**

COORDINATORE: **PROF. PATRIZIA LONGOBARDI**

TUTOR: **PROF. CIRO D'APICE**
CO-TUTOR: **DOTT.SSA ROSANNA MANZO**

Anno Accademico 2011 – 2012

Contents

List of Figures

Introduction

In the last decades, the modeling of crowd motion and pedestrian flow has attracted the attention of applied mathematicians, because of an increasing number of applications, in engineering and social sciences, dealing with this or similar complex systems, for design and optimization purposes.

The crowd has caused many disasters, in the stadiums during some major sporting events as the "Hillsborough disaster" occurred on 15 April 1989 at Hillsborough [5], a football stadium, in Sheffield, England, resulting in the deaths of 96 people, and 766 being injured that remains the deadliest stadium-related disaster in British history and one of the worst ever international football accidents. Other example is the "Heysel Stadium disaster" occurred on 29 May 1985 (see [4]) when escaping, fans were pressed against a wall in the Heysel Stadium in Brussels, Belgium, as a result of rioting before the start of the 1985 European Cup Final between Liverpool of England and Juventus of Italy. Thirty-nine Juventus fans died and 600 were injured. It is well know the case of the London Millennium Footbridge, that was closed the very day of its opening due to macroscopic lateral oscillations of the structure developing while pedestrians crossed the bridge (cf. Dallard et al. [17]). This phenomenon renewed the interest toward the investigation of these issues by means of mathematical modeling techniques (see Venuti et al. [33] and the main references therein). Other examples are emergency situations in crowded areas as airports or railway stations. In some cases, as the pedestrian disaster in Jamarat Bridge located in South Arabia, mathematical modeling and numerical simulation have already been successfully employed to study the dynamics of the flow of pilgrims, so as to highlight critical circumstances under which crowd accidents tend to occur and suggest counter-measures to improve the safety of the event (Helbing et al. [21], Hughes [24]).

In the existing literature on mathematical modeling of human crowds we can distinguish two approaches: microscopic and macroscopic models. In model at microscopic scale pedestrians are described individually in their motion by ordinary differential equations and problems are usually set in two-dimensional domains delimiting the walking area under consideration, with the presence of obstacles within the domain and a target. The basic modeling framework relies on classical Newtonian laws of point (Helbing and Johansson [19], Maury and Venel [26]). The model at the macroscopic scale consists in using partial differential equations, that is in describing the evolution in time and space of pedestrians supplemented by either suitable closure relations linking the velocity of the latter to their density (see e.g., Hughes [24]) or analogous balance law for the momentum (see e.g., Bellomo and Dogbé [6]). Again, typical guidelines in devising this kind of models are the concepts of preferred direction of motion and discomfort at high densities. In the framework of scalar conservation laws, a macroscopic onedimensional model has been proposed by Colombo and Rosini [11], resorting to some common ideas to vehicular traffic modeling, with the specific aim of describing the transition from normal to panic conditions. Piccoli and Tosin [31] propose to adopt a different macroscopic point of view, based on a measure-theoretical framework which has recently been introduced by Canuto et al. [8] for coordination problems (rendezvous) of multiagent systems. This approach consists in a discrete-time Eulerian macroscopic representation of the system via a family of measures which, pushed forward by some motion mappings, provide an estimate of the space occupancy by pedestrians at successive time steps. From the modeling point of view, this setting is particularly suitable to treat nonlocal interactions among pedestrians, obstacles, and wall boundary conditions.

A microscopic approach is advantageous when one wants to model differences among the individuals, random disturbances, or small environments. Moreover, it is the only reliable approach when one wants to track exactly the position of a few walkers. On the other hand, it may not be convenient to use a microscopic approach to model pedestrian flow in large environments, due to the high computational effort required. A macroscopic approach may be preferable to address optimization problems and analytical issues, as well as to handle experimental data. Nonetheless, despite the fact that self-organization phenomena are often

visible only in large crowds [19], they are a consequence of strategical behaviors developed by individual pedestrians.

The two scales may reproduce the same features of the group behavior, thus providing a perfect matching between the results of the simulations for the microscopic and the macroscopic model in some test cases. This motivated the multiscale approach proposed by Cristiani, Piccoli and Tosin [14]. Such an approach allows one to keep a macroscopic view without losing the right amount of "granularity," which is crucial for the emergence of some self-organized patterns. Furthermore, the method allows one to introduce in a macroscopic (averaged) context some microscopic effects, such as random disturbances or differences among the individuals, in a fully justifiable manner from both the physical and the mathematical perspective. In the model, microscopic and macroscopic scales coexist and continuously share information on the overall dynamics. More precisely, the microscopic part tracks the trajectories of single pedestrians and the macroscopic part the density of pedestrians using the same evolution equation duly interpreted in the sense of measures. In this respect, the two scales are indivisible.

Starting from model of Cristiani, Piccoli and Tosin we have implemented algorithms to simulate the pedestrians motion toward a target to reach in a bounded area, with one or more obstacles inside. In this work different scenarios have been analyzed in order to find the obstacle configuration which minimizes the pedestrian average exit time. The optimization is achieved using to algorithms. The first one is based on the exhaustive exploration of all positions: the average exit time for all scenarios is computed and then the best one is chosen. The second algorithm is of steepest descent type according to which the obstacle configuration corresponding to the minimum exit time is found using an iterative method. A variant has been introduced to the algorithm so to obtain a more efficient procedure. The latter allows to find better solutions in few steps than other algorithms. Finally we performed other simulations with bounded domains like a classical flat with five rooms and two exits, comparing the results of three different scenario changing the positions of exit doors.

The thesis is organized as follow. Chapter 1 reports the state of the art about the existing literature on mathematical modeling of human crowds. Chapter 2 deal with the multiscale model of Cristiani, Piccoli and Tosin. A numerical ap-

proximation of the model equations with special emphasis on the discretization in space of the macroscopic scale is proposed in Chapter 3. Finally Chapter 4 is devoted to the results of numerical simulations and to their discussion.

Chapter 1

State of the art

In the existing literature on mathematical modeling of human crowds we can distinguish two approaches: microscopic and macroscopic models. In model at microscopic scale pedestrians are described individually in their motion by ordinary differential equations and problems are usually set in two-dimensional domains delimiting the walking area under consideration, with the presence of obstacles within the domain and a target. The basic modeling framework relies on classical Newtonian laws of point (Helbing and Johansson [19], Maury and Venel [26]). The model at the macroscopic scale consists in using partial differential equations, that is in describing the evolution in time and space of pedestrians supplemented by either suitable closure relations linking the velocity of the latter to their density (see e.g., Hughes [6]) or analogous balance law for the momentum (see e.g., Bellomo and Dogbé [6]).

1.1 A microscopic approach by Helbing et al.

Even if the pedestrian flow can show a chaotic appearance, one can find regularities in individual pedestrian behavior. (1) Pedestrians normally choose the fastest route to their next destination which has therefore the shape of a polygon. If alternative routes are of the same length, a pedestrian prefers the one where he or she can go straight ahead for as long as possible and change direction as late as possible (provided that the alternative route is not more attractive, for example, because of less noise, more light, a friendlier environment, less waiting

time at traffic lights, etc). This behavior sometimes produces 'hysteresis effects'; that is, at some locations, pedestrians tend to use a typical way to a certain point, but another way back. (2) Pedestrians prefer to walk with an individual desired speed, which corresponds to the most comfortable walking speed so long as it is not necessary to go faster in order to reach the destination in time. The desired speeds within pedestrian crowds are Gaussian distributed. (3) Pedestrians keep a certain distance from other pedestrians and borders (of streets, walls, and obstacles). This distance is smaller as the pedestrian hurries, and it also decreases with growing pedestrian density. Resting individuals (waiting on a railway platform for a train, sitting in a dining hall, or lying at a beach) are uniformly distributed over the available area if there are no acquaintances among the individuals. Pedestrian density increases (that is, interpersonal distances lessen) around particularly attractive places, and it decreases with growing velocity variance. Individuals who know each other may form groups which are entities that behave in a manner similar to single pedestrians. (4) Pedestrians normally do not reflect their behavioral strategy in every situation anew but act more or less automatically (as an experienced car driver does). This becomes obvious when pedestrians cause delays or obstructions, for example, by entering an elevator or train even though others are still trying to get off. Additionally, at medium and high pedestrian densities, the motion of pedestrian crowds shows some striking similarities with the motion of gases and fluids.

(a) Footsteps of pedestrians in snow look similar to streamlines of fluids.

(b) At borderlines between opposite directions of walking one can observe 'viscous fingering'.

(c) When stationary pedestrian crowds need to be crossed, the moving pedestrians form river-like streams (see figure 1.1).

(d) The propagation of shock waves can be found in dense pedestrian crowds which push forward.

Apart from these phenomena, there are some similarities with granular flows (in figure 1.1, the long-exposure photograph of a stationary crowd in front of a cinema shows that crossing pedestrians form a river-like stream.).

Assuming that pedestrians behave according to the optimal strategy (which is normally a good approximation but less true for children and tourists) it can

Figure 1.1: Stationary crowd in front of a cinema

still not predict the spatiotemporal movement of a single pedestrian. This is not only due to behavioral variations ('fluctuations' in behavior), but also because they usually do not know the destinations and preselected route of a pedestrian. Nevertheless it is possible to predict pedestrian streams with a surprisingly high accuracy.

The positions of the pedestrians α can be represented by points $r_\alpha(t)$ in space, which change continuously over time t, and pedestrians dynamics can be described by the following equation of motion:

$$\frac{dr_\alpha(t)}{dt} = v_\alpha(t).$$

The functions delineating the temporal changes of the actual pedestrian velocities $v_\alpha(t)$ can be interpreted as the driving forces of this motion, which are called *behavioral forces or social forces.*

If the behavioral force $f_\alpha(t)$ represents the different systematic influences (of the environment and other pedestrians) on the behavior of a pedestrian α, and the fluctuation term $\xi_\alpha(t)$ reflects random behavioral variations (arising from accidental or deliberate deviations from the optimal strategy of motion), the following is

the *equation of acceleration*:

$$\frac{dv_\alpha}{dt} = f_\alpha(t) + \xi_\alpha(t).$$

The behavioral force $f_\alpha(t)$ is the sum of several force terms which correspond to the different influences simultaneously affecting the behavior of pedestrian α:

$$f_\alpha(t) = f_\alpha^0(v_\alpha) + f_{\alpha B}(r_\alpha) + \sum_{\beta(\neq\alpha)} f_{\alpha\beta}(r_\alpha, v_\alpha, r_\beta, v_\beta) + \sum_i f_{\alpha i}(r_\alpha, r_i, t) + \xi_\alpha(t)$$

where

- $f_\alpha^0(v_\alpha)$ is a correction, within the so-called relaxation time τ_α, of deviation's disturbance of the actual velocity v_α from desired velocity v_α^0. The desired velocity is the standard velocity in the direction e_α of his or her next destination.

$$f_\alpha^0(v_\alpha) = \frac{1}{\tau_\alpha}(v_\alpha^0 e_\alpha - v_\alpha). \tag{1.1}$$

- $f_{\alpha B}$ is a repulsive force of borders which decreases monotonically with the distance $||r_\alpha - r_\beta^\alpha||$ between the place r_α of pedestrian α and nearest point r_β^α of the border.

- $f_{\alpha\beta}(r_\alpha, v_\alpha, r_\beta, v_\beta)$ is a repulsive force term, used to indicate that each pedestrian α keeps a situation-dependent distance from the other pedestrians β.

- $f_{\alpha i}(r_\alpha, r_i, t)$ is an attractive force an opposite sign and a longer range of interactions respect to the repulsive force.

Some observations, reported in point (3), can be easily explained by looking at equilibria between certain behavioral forces, for which the acceleration vanishes. In the absence of special attractions, the positions r_α of the pedestrians follow form:

$$\sum_{\beta(\neq\alpha)} f_{\alpha\beta}(r_\alpha, 0, r_\beta, 0) = 0 \tag{1.2}$$

A classical example in which the velocity $v_\alpha = 0$ is represented by pedestrians waiting on a railway platform, sitting in a restaurant, or lying on a beach.

In case of additional attraction effects $f_{\alpha i}$ (such as the stage in a rock concert), equation (1.18) must be supplemented by the corresponding forces of attraction:

$$\sum_{\beta(\neq\alpha)} f_{\alpha\beta}(r_\alpha, 0, r_\beta, 0) + \sum_i f_{\alpha i}(r_\alpha, r_i) = 0$$

Focusing on situations where a pedestrian α cannot overtake a slower pedestrian β moving with velocity v_β, it have to set up the equation for the equilibrium between the acceleration force f_α^0 and the repulsive force $f_{\alpha\beta}$. Because $v_\alpha = v_\beta$, this yields:

$$\frac{1}{\tau_\alpha}(v_\alpha^0 e_\alpha - v_\beta) + f_{\alpha\beta}(r_\alpha, v_\beta, r_\beta, v_\beta) = 0$$

where the actual velocity v_β, the distance vector $(r_\beta - r_\alpha)$, and the repulsive force $f_{\alpha\beta}$ point in the desired direction e_α of walking. they therefore have:

$$\frac{v_\alpha^0 - v_\beta}{\tau_\alpha} + f_{\alpha\beta}(r_\alpha, e_\alpha v_\beta, r_\alpha + \Delta r_{\alpha\beta} e_\alpha, v_\beta e_\alpha) = 0$$

where τ_α denotes the 'acceleration time' to reach the desired velocity, so that $(v_\alpha^0 - v_\beta)/\tau_\alpha$ reflects the acceleration strength. From this formula (and remembering that the repulsive force increases with decreasing distance) it can be seen that pedestrians keep a smaller distance $\Delta r_{\alpha\beta} = ||r_\alpha - r_\alpha||$, the larger the difference between their own desired velocity v_α^0 and the speed v_β of the preceding pedestrian. This corresponds to the well-known pushing behavior of pedestrians. Combined with the growth of the desired speed owing to delays, an interesting phenomenon is observed in pedestrian queues, as illustrated by figure 1.2. When the front of a queue (top) is stopped, one can often observe. After that some time, one of the waiting pedestrians begins to move forward a little bit, because his or her desired velocity grows, leading to a smaller equilibrium distance to the pedestrian in front. This causes the successor to follow up and so forth, leading to a wave-like propagation of the gap to the end of the queue and to a compaction of

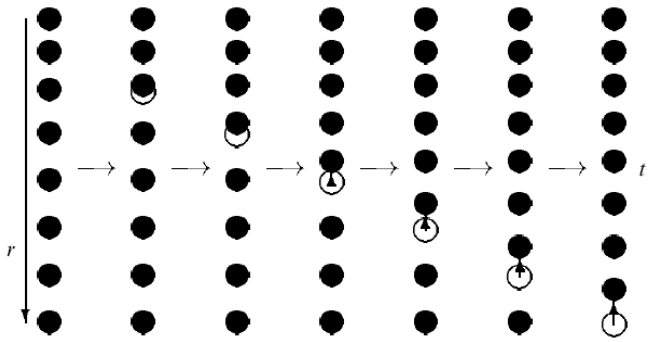

Figure 1.2: Pedestrian queue phenomenon.

the queue. Thereby, the tendencies of all individuals to move forward a little add up towards the end of the queue, giving rise to larger following-up distances.

How long a pedestrian joins an attraction at place r_i is calculated by looking at the equilibrium between the acceleration force f_α^0 and an attracting force $f_{\alpha i}$:

$$\frac{v_\alpha^0(t)e_\alpha - 0}{\tau_\alpha} + f_{\alpha i}(r_\alpha, r_i, t) = 0.$$

Equilibrium considerations are also useful for specifying the model parameters appropriately, because certain plausibility criteria must be met. For example, pedestrians should normally not move opposite to their desired walking directions. This implies that:

$$\frac{v_\alpha^0}{\tau_\alpha} \approx \frac{v_\beta^0}{\tau_\beta}.$$

The behavioral force model of pedestrian dynamics has been simulated for a large number of interacting pedestrians confronted with different situations. Under certain conditions the self-organization of collective behavioral patterns can be found, just as in some related models of bird swarms (Reynolds, 1987; Vicsek et al, 1995). 'Self-organization' means that these patterns are not externally planned, prescribed, or organized, for example, by traffic signs, laws, or behavioral conventions. Instead the spatiotemporal patterns emerge through the nonlinear interactions of pedestrians. The model oh Helbing et al. (according to which

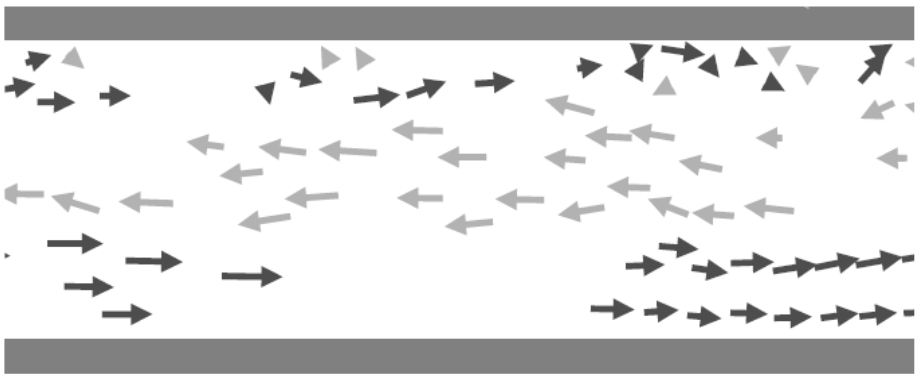

Figure 1.3: Formation of lanes

individuals behave somewhat automatically) can explain the self-organized patterns described below without assuming strategic considerations, communication, or the imitative behavior of pedestrians. All these collective patterns of motion are symmetry-breaking phenomena, although the model was formulated completely symmetrically with respect to the right-hand and left-hand sides. In follows we report some interesting phenomenon captured by Helbing et al. simulazions.

(1) The model reproduce the empirically observed formation of lanes consisting of pedestrians with the same desired walking direction (see figure 1.3). In crowds of oppositely moving pedestrians, one can observe the formation of varyinglanes consisting of pedestrians with the same desired direction of motion. This is also the case if interacting pedestrians avoid each other with the same probability on the right-hand side and on the left-hand side. The reason for lane formation is the related decrease in the frequency of necessary deceleration and avoidance maneuvers, which increases the efficiency of the pedestrian flow. (The positions, directions, and lengths of the arrows represent the places, walking directions, and speeds of pedestrians.). These lanes are dynamically varying. Their number depends on the width of the street and on pedestrian density.

In the conventional interpretation of lane formation, it is assumed that pedestrians tend to walk on the side which is prescribed in vehicular traffic. However, this model can explain lane formation even without assuming a preference for any side. The mechanism of lane formation can be understood as follows: pedestrians moving against the stream or in areas of mixed directions of motion will have fre-

quent and strong interactions. In each interaction, the encountering pedestrians move a little aside in order to pass each other. This sidewards movement tends to separate oppositely moving pedestrians. Moreover, pedestrians moving in uniform lanes will have very rare and weak interactions. Hence the tendency to break up existing lanes is negligible, when the fluctuations are small. Furthermore, the most stable configuration corresponds to a state with a minimal interaction rate and is related to a maximum efficiency of motion.

Note that, at sufficiently high pedestrian densities, lanes are destroyed by increasing the fluctuation strength (which is analogous to the temperature). This gives rise to the formation of blocked situations, which may even have a regular (that is, 'crystallized' or 'frozen') structure. This surprising transition called 'freezing by heating' and believe that it is relevant to situations involving pedestrians under extreme conditions (panics): Imagine a very smoky situation, caused by fire, in which people do not know which is the right way to escape. In figure 1.4 the ensemble-averaged efficiency $\langle E \rangle$ of the system as a function of the particle number N and the noise intensity Θ on a logarithmic scale. Shown above are averages over twenty-five simulation runs with different random seeds. The decrease in efficiency from values close to 1 to values around 0 with increasing fluctuation intensity Θ but a constant number N of particles indicates the transition from the fluid to the crystallized state that we call 'freezing by heating'. When panicking, people will just try to get ahead, with a reduced tendency to follow a certain direction. Thus fluctuations will be very large, which can lead to fatal blockages. As a consequence, models for everyday pedestrian streams are not suitable for the realistic simulation of emergency situations. The latter requires simulations with modified parameter sets corresponding to less optimal pedestrian behavior. In particular, the fluctuation strength is considerably higher for panic situations than for usual conditions.

(2) In Helbing et al. simulations of narrow passages, they observed oscillatory changes in the walking direction. In figure 1.5 at narrow passages one finds an oscillation of the passing direction. When a pedestrian is able to pass through the door, normally another pedestrian can follow him or her easily (above). However, the pedestrian stream arising in this way will stop after some time owing to the pressure from the other side of the passage. Some time later, a pedestrian

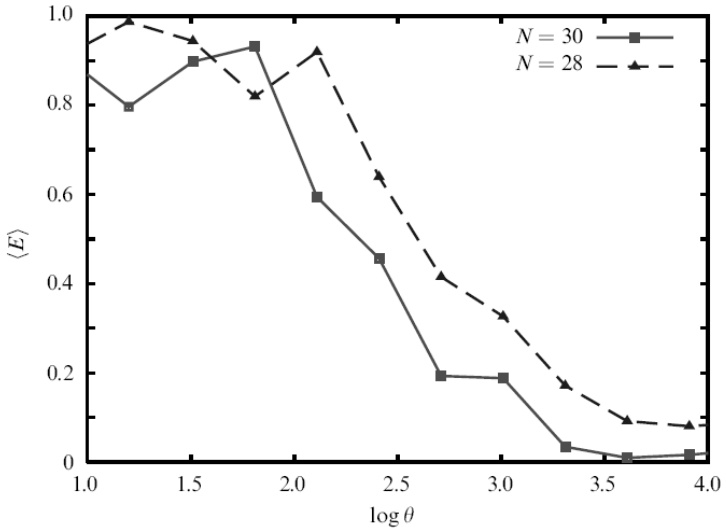

Figure 1.4: Freezing by heating.

will pass through the door in the opposite direction, and the process continues as outlined before (below).. The conventional interpretation for a change in the walking direction is that, after some time, a pedestrian gives precedence to a waiting pedestrian walking in the opposite direction. This cannot, however, explain the increase in oscillation frequency with passage width. The mechanism leading to alternating flows is as follows: once a pedestrian is able to pass the narrowing (door, staircase, etc), pedestrians with the same walking direction can easily follow, which is particularly clear for long passages. In this way, the number and 'pressure' of waiting and pushing pedestrians becomes less than on the other side of the narrowing where, consequently, the chance to occupy the passage grows. This leads to a deadlock situation after some time which is followed by a change in the walking direction. Capturing the passage is easier if it is broad and short so that the walking direction changes more frequently.

(3) At intersections the simulations show the temporary emergence of unstable round-about traffic. In figure 1.6 see the phases of temporary roundabout traffic (above) alternate with phases during which the intersection is crossed in the 'vertical' or the 'horizontal' direction. The efficiency of pedestrian flow can be increased considerably by putting an obstacle in the center of the intersection,

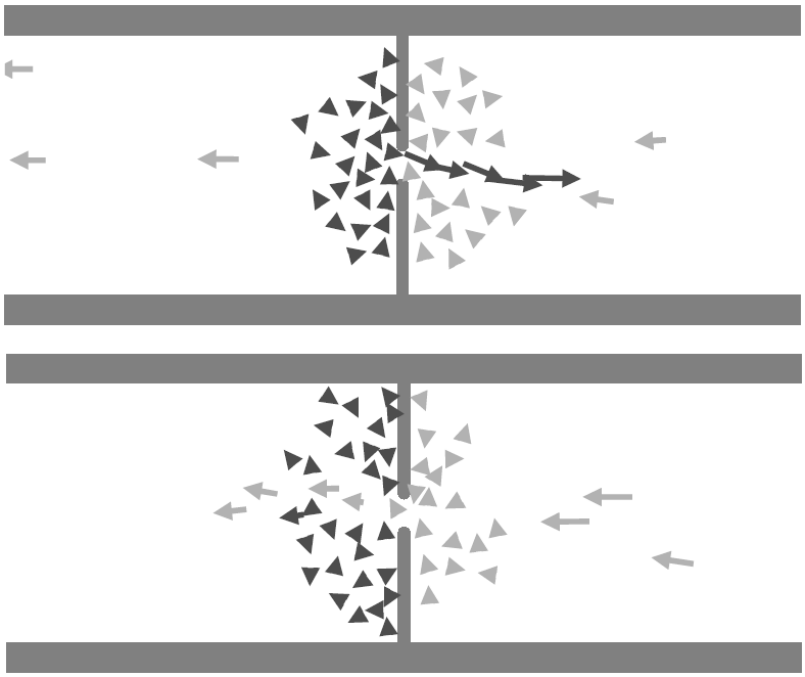

Figure 1.5: Example of simulation.

because this favors the smooth roundabout traffic compared with the competing, inefficient patterns of motion.. This is similar to the emergent rotation in the case of self-driven particles. However, the rotation direction of circular pedestrian flows is alternating. Roundabout traffic is connected with small dettheirs but decreases the frequency of necessary deceleration, stopping, and avoidance maneuvers considerably, so that pedestrian motion becomes more efficient on average.

1.2 A macroscopic approach by Colombo and Rosini

The starting print of Colombo and Rosini approach is the classical Lighthill Whitam and Richards (LWR) model, introduced with reference to car flows but referred to also in the case of pedestrians. The LWR model reads:

$$\partial_t \rho + \partial_x q(\rho) = 0 \tag{1.3}$$

with flow function $\rho \to q(\rho) = \rho v(\rho)$ throughly (see Figure 1.7). Here, $\rho \in [0, R]$ is the pedestrian density, R is the maximal density and $v = v(\rho)$ is the pedestrian

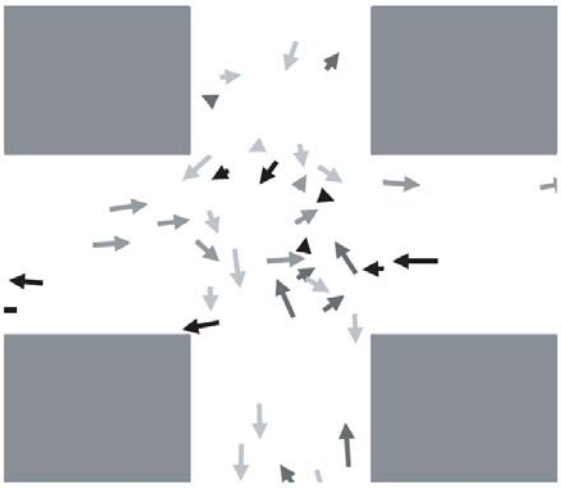

Figure 1.6: Motion which are very short-lived and unstable

speed. The simplicity of this model stems from its being the consequence of only two assumptions:

(C) Conservation: the total number of pedestrians is constant

(SL) Speed Law: v is a function of ρ.

Denote by ρ_0 an initial datum for (1.20), say $\rho_0 \in L^1(\mathbb{R}; [0, R])$, by $\rho = \rho(t, x)$ the corresponding solution and fix two constants $\rho_{\min}, \rho_{\max}$, with $0 < \rho_{\min}$

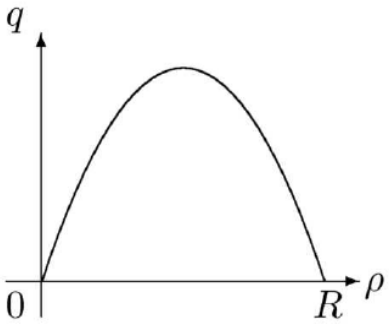

Figure 1.7: Typical flow for the LWR model.

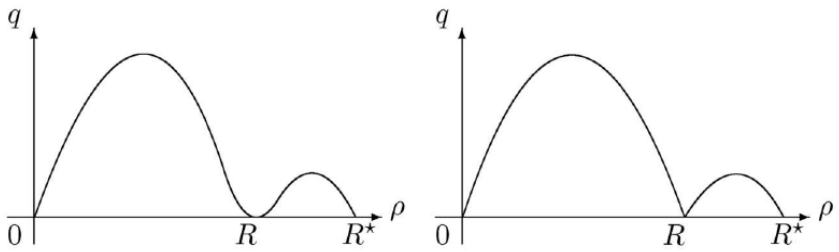

Figure 1.8: Two possible flow functions satisfying (**Q**).

$< \rho_{\max} < R$. A major problem in using conservation laws in the modeling of pedestrian flow is the *"maximum principle"*:

(MP) If the initial distribution ρ_0 satisfies the bounds $\rho_0(x) \in [\rho_{\min}, \rho_{\max}]$ for all $x \in R$, then the corresponding solution satisfies the same bounds for all times, i.e. $\rho(t, x) \in [\rho_{\min}, \rho_{\max}]$ for all $t \geq 0$ and $x \in \mathbb{R}$.

The model introduced below is based on the same two assumptions **(C)** and **(SL)** of the LWR model. However, Colombo and Rosini modified the speed law (or, equivalently, the fundamental diagram) and, what is most relevant, the very definition of solution. Introduce a further characteristic density, say R^*, having the role of the maximal density in exceptional situations (panic). The speed law chosen an such way that the density flow diagram is as in Figure 1.8.

Under usual circumstances, ρ varies in $[0, R]$. The rise of panic, caused for instance by a sharp increase in the density, forces ρ to enter the interval $[R, R^*]$. More precisely, introduces the following assumptions on the flow q (see Figure 1.9).

(Q) $q : [0, R^*] \to [0, +\infty[$ is smooth, say $C^0([0, R^*]) \cap C^2([0, R^*] \backslash \{R\})$, and moreover

1. $q(\rho) = 0$ iff $\rho \in \{0, R, R^*\}$.
2. q' is bounded on $[R, R^*]$. In $]0, R[$, q' vanishes at a single point R_M. Similarly, in $]R, R^*[$, q' vanishes at a single point R^*_M.
3. q has at most one inflection point R_I in $]R_M, R[$, at most another one R^*_I in $]R, R^*_M[$ and no other inflection point.

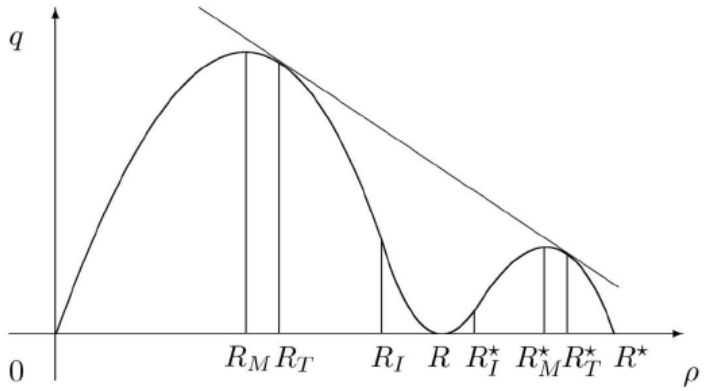

Figure 1.9: Notation for extreme and inflection points.

The above assumptions are meant to consider also the case in which q' is not defined at R, see Figure 1.8, right. Assumes that $q \in C^2$. Nonclassical solutions to scalar conservation laws has been adopted. More precisely, a solution to can be constructed by means of solutions to Riemann problems. Recall that a Riemann problem is a Cauch problem of this type:

$$\begin{cases} \partial_t \rho + \partial_x q(\rho) = 0 \\ \rho(0,x) = \begin{cases} \rho^l \text{ if } x < 0, \\ \rho^r \text{ if } x \geq 0, \end{cases} \end{cases} \tag{1.4}$$

Nonclassical solutions satisfy (1.4) in its weak (or integral) form, but may well violate the other usual admissibility conditions found in the literature, such as Lax inequalities, the vanishing viscosity criterion or the various entropy conditions. In other words, a nonclassical shock is a discontinuity that satis es the Rankine-Hugoniot conditions, but not necessarily also Liu's entropy condition. Heading towards a definition of the solution $\Re(\rho^l, \rho^r)$ to (1.4) for all $\rho^l, \rho^r \in [0, R^*]^2$, a key issue is defining when a Riemann problem leads to a classical solution and when to a nonclassical one. Recall, that by Riemann Solver they mean a map that to any pair (ρ^l, ρ^r) in $[0, R^*]^2$ associates a weak, self-similar solution to (1.4) computed at time, say, $t = 1$. As it is usual when dealing with nonclassical scalar conservation laws, it introduce auxiliary functions to describe tangents to the fundamental diagram are defined.

Introduce the continuous function φ implicitly defined by:

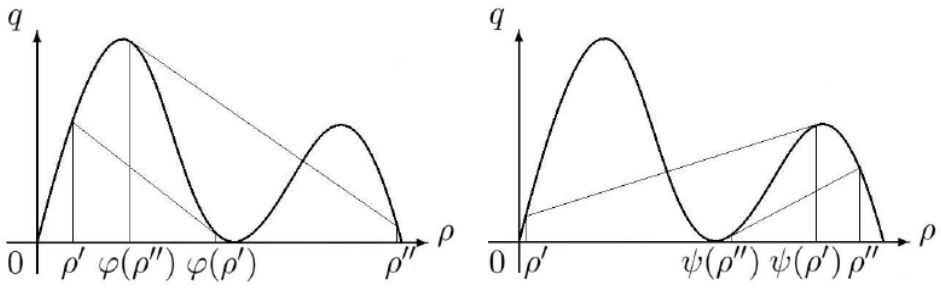

Figure 1.10: Constructions of ψ and φ.

$$\varphi : [0, R^*] \rightarrow [0, R]$$
$$\rho \rightarrow \begin{cases} r \text{ such that } q'(r) = \frac{q(r)-q(\rho)}{r-\rho} & \text{if } r \text{ exist,} \\ R_I & \text{if } \rho = R_I, \\ 0 \text{ or } R^* & \text{otherwise.} \end{cases}$$

The analogous continuous map ψ attaining values in $[R, R^*]$ is defined by:

$$\psi : [0, R^*] \rightarrow [R, R]$$
$$\rho \rightarrow \begin{cases} r \text{ such that } q'(r) = \frac{q(r)-q(\rho)}{r-\rho} & \text{if } r \text{ exist,} \\ R_I^* & \text{if } \rho = R_I^*, \\ R \text{ or } R^* & \text{otherwise.} \end{cases}$$

Finally, define also:

$$\Phi : [0, R] \rightarrow [0, R]$$
$$\rho \rightarrow \begin{cases} r : \frac{q(r)-q(\rho)}{r-\rho} = \frac{q(\rho)-q(\psi(\rho))}{\rho-\psi(\rho)} & \text{if } r \text{ exist,} \\ \rho & \text{otherwise.} \end{cases}$$

Let φ be such that the straight line through $(\rho, q(\rho))$ and $(\varphi(\rho), q(\varphi(\rho)))$ is tangent to $q = q(\rho)$ in $(\varphi(\rho), q(\varphi(\rho)))$ and $\varphi(\rho) \in [0, R]$, if it exists (see Figure 1.10, left). Similarly, let ψ be such that the straight line through $(\rho, q(\rho))$ and $(\psi(\rho), q(\psi(\rho)))$ is tangent to $q = q(\rho)$ in $(\psi(\rho), q(\psi(\rho)))$ and $\psi(\rho) \in [R, R^*]$ (see

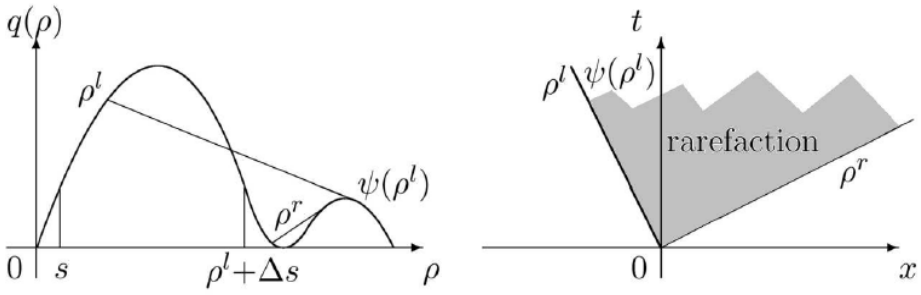

Figure 1.11: A nonclassical solution described in (R1).

Figure 1.10, right). The line through $(\rho, q(\rho))$ and $(\varphi(\rho), q(\varphi(\rho)))$ may have a further intersection with the curve $q = q(\rho)$, which they call $(\Phi(\rho), q(\Phi(\rho)))$.

They are now able to define a Riemann solver $\Re$. Fix two positive thresholds s and Δs such that $s + \Delta s < R$. Consider first the case in which ρ^l and ρ^r are in $[0, R]$.

(R1) If ρ^l,$\rho^r \in [0, R]$ then $\Re(\rho^l, \rho^r)$ selects the classical solution unless $\rho^l \geq s, \rho^r \geq \Phi(\rho^l)$ and $\rho^r - \rho^l > \Delta s$. In this case, $\Re(\rho^l, \rho^r)$ consists of a nonclassical shock between ρ^l and $\psi(\rho^l)$, followed by the classical solution of the Riemann problem with states $\psi(\rho^l)$ and ρ^r.

This solution is described in figures 1.11 (with standard initial data but leading to panic states) and 1.12 (the classical solution would consist of a single shock.). Its physical interpretation is as follows. Fix ρ^l,$\rho^r \in [0, R]$. If ρ^l is *"very low"*, i.e. below s, then panic may not arise, independently from $\rho^r \in [0, R]$. Similarly, if $\rho^r - \rho^l$ is *"very low"*, i.e. $\rho^r - \rho^l < \Delta s$, then pedestrians are ready to stand the increase in the density without panicking. On the contrary, when the pedestrian density ρ^l is above the first threshold s and also ρ^r is *"high"*, then a *"suffciently high"* density increase causes panic, leading to the formation of a pedestrian jam, i.e. of an area where the density is greater than the usual maximum R. Here, is implied *"suffciently high"* mean above Δs the condition $\rho^r > \Phi(\rho^l)$ is implied by $\rho^r - \rho^l > \Delta s$ as soon $\Delta s > \Phi(0)$. Remark that the map $\rho^l \to \Phi(\rho^l)$ is a decreasing function of ρ^l and $\Phi(s) < R$. Indeed, the higher ρ^l, the easier is the transition from ρ^l to a panic state.

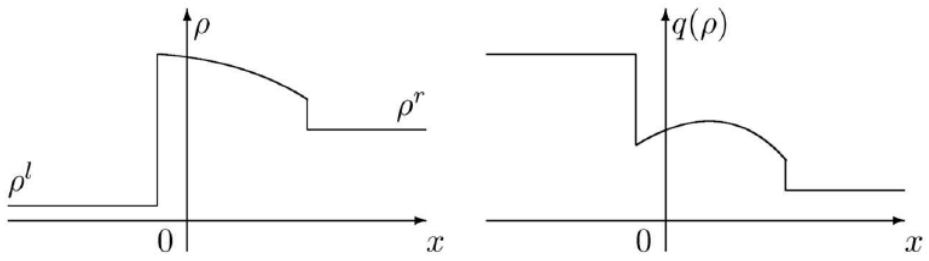

Figure 1.12: Solution to (1.4) at time $t = 1$ in case (R1).

They now extend the definition of the solution to (1.4) to all cases $(\rho^l, \rho^r) \in [0, R^*]^2$. First, they impose that:

(R2) If $\rho^r < \rho^l$, then $\Re(\rho^l, \rho^r)$ is the classical solution.

The above condition means that when people face a density lower than the one they are in, then panic does not arise. Finally, in the remaining cases, they pose:

(R3) if $\rho^r > R$ and $\rho^r > \rho^l$, then $\Re(\rho^l, \rho^r)$ consist of a nonclassical shock between ρ^l and a panic state followed by, possibly null, classical waves. More precisely,

$\rho^r \in]R, \psi(\rho^l)]$: $\Re(\rho^l, \rho^r)$ consists of a nonclassical shock between ρ^l and $\psi(\rho^l)$, followed by classical waves;

$\rho^r \in [\psi(\rho^l), R^*[$: $\Re(\rho^l, \rho^r)$ consists of a single shock.

The above properties (R1), (R2) and (R3) uniquely determine a Riemann solver R defined on all $[0, R^*]^2$.

To state it, the following subsets of the square $[0, R^*]^2$ are of use, see Figure 1.13 (left, in the case $s + \Delta s > \Phi(0, \psi(0))$ and, right, in the general case.).

Qualitative properties

Consider the well known situation of a group of people that need to leave a corridor through a door. If the maximal outflow allowed by the door is low, then the transition to panic in the crowd approaching the door may well cause a dramatic reduction in the real outflow, making it even lower than that usually allowed by the door.

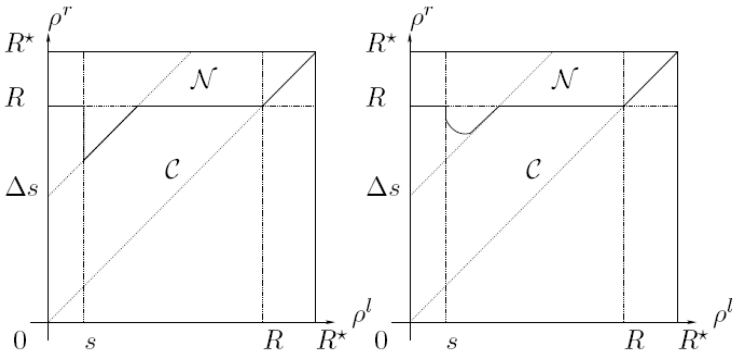

Figure 1.13: The Riemann Solver.

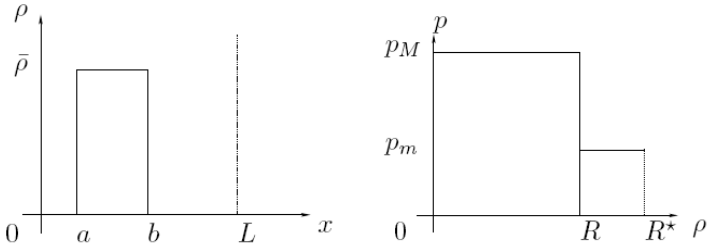

Figure 1.14: Left, the initial datum and, right, the maximal outflow in (1.5)

More precisely, choose a flow as in Figure 1.8, left. Assume that the corridor is the half line $]-\infty, L]$. The crowd is initially uniformly distributed on $[a, b]$ with uniform density $\overline{\rho}$, with $0 < a < b < L$ and $\overline{\rho}$, see Figure 1.14, left. This situation is analytically described by

$$\begin{cases} \partial_t \rho + \partial_x q(\rho) = 0 & (t, x) \in [0, +\infty[\, x \,]-\infty, L], \\ \rho(0, x) = \overline{\rho} \cdot \chi_{[a,b]}(x) & x \in]-\infty, L[, \\ q(\rho(t, L)) \leq p(\rho(t, L)) & t \in [0, \infty[. \end{cases} \tag{1.5}$$

Here, $p : [0, R^*] \to [0, +\infty[$ represents the given maximal possible outflow through the door at $x = L$. This outflow is significantly affected by the crowd density. Therefore, they choose the simple piecewise constant behavior in Figure 1.14, right. Here, p_M is the outflow in standard (i.e. not overcompressed) situation, while p_m denotes the same quantity in the overcompressed regime. Assume $0 < p_m < p_M$. (1.5) is an initial boundary value problem. The analytical treatment of

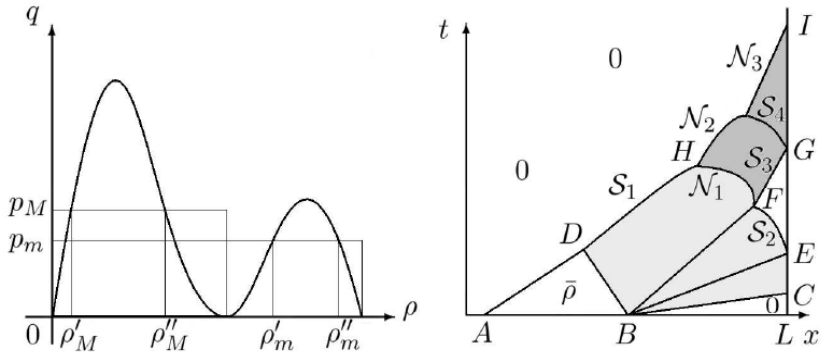

Figure 1.15: Construction of the solution to (1.5).

this and of the Cauchy problem is deferred to [3], where the existence of solutions and their continuous dependence from time is proved. Some qualitative properties of the solution to (1.5) constructed through wave front tracking are shown. The aim is to show how the present model describes the "*overcompression*" effect due to the rise of panic and the consequent fall in the outflow.

While the overall picture of the solution to (1.5) is rather stable, a detailed analytical study necessarily needs to consider many slightly different cases. Below, they restrict the construction of the solution of (1.5) to the most representative situations in which panic arises is considered.

With reference to (1.5) and Figure 1.15 (the light shaded areas on the right display rarefactions, while the darker ones represent areas where people are in panic states), left, call $\rho'_M, \rho''_M, \rho'_m, \rho''_m$ densities such that

$$\begin{aligned} \rho'_M, \rho''_M &\in]0, R[, \rho'_M < \rho''_M, \rho_M = q(\rho'_M) = q(\rho''_M), \\ \rho'_m, \rho''_m &\in]R, R^*[, \rho'_m < \rho''_m, \rho_m = q(\rho'_m) = q(\rho''_m). \end{aligned}$$

Assume that the door is small, in the sense that its outflow satisfies

$$\rho_M < q(R^*_M), \rho_M < q(s), \rho_M < q(s + \Delta s), \rho_m < \rho_M \tag{1.6}$$

and the initial amount of people is suitably large:

$$(b - a)\overline{\rho} > (L - b) \left(\frac{1}{q'(\rho'_M)} - \frac{1}{q'(0)} \right) p_M. \tag{1.7}$$

The first step in the construction is to consider the Riemann problems

$$\begin{cases} \partial_t \rho + \partial_x q(\rho) = 0 \\ \rho(0,x) = \begin{cases} 0 \text{ if } x < a, \\ \overline{\rho} \text{ if } x \geq a, \end{cases} \end{cases} \quad \begin{cases} \partial_t \rho + \partial_x q(\rho) = 0 \\ \rho(0,x) = \begin{cases} \overline{\rho} \text{ if } x < b, \\ 0 \text{ if } x \geq b. \end{cases} \end{cases} \tag{1.8}$$

The former is solved by a classical shock. The latter is solved by a rarefaction wave if $\overline{\rho} \in]0, R_I]$, or by a classical shock between states $\overline{\rho}$ and $\varphi(\overline{\rho})$, followed by a rarefaction from $\varphi(\overline{\rho})$ to zero if $\overline{\rho} \in]R_I, R]$. Therefore, for small times, the solution to (1.5) in the case $\overline{\rho} \in]R_I, R]$, is

$$\begin{cases} 0 & \text{if } x \in]-\infty, a + [q(\overline{\rho})/\overline{\rho}]t[, \\ \overline{\rho} & \text{if } x \in]a + [q(\overline{\rho})/\overline{\rho}]t, b + q'(\overline{\rho})t[, \\ \rho & \text{if } x = b + q'(\rho)t, \\ 0 & \text{if } x \in]b + q'(0)t, L[. \end{cases} \tag{1.9}$$

while if $\rho \in]R_I, R[$,

$$\begin{cases} 0 & \text{if } x \in]-\infty, a + [q(\overline{\rho})/\overline{\rho}]t[, \\ \overline{\rho} & \text{if } x \in]a + [q(\overline{\rho})/\overline{\rho}]t, b + q'(\varphi(\overline{\rho}))t[, \\ \varphi(\overline{\rho}) & \text{if } x = b + q'(\varphi(\overline{\rho}))t, \\ \rho & \text{if } x = b + q'(\rho)t, \\ 0 & \text{if } x \in]b + q'(0)t, L[. \end{cases}$$

Assume that $\rho \in]0, R_I]$, the other case being essentially analogous.

Note that pedestrians start exiting through the door at time $t_c = (L-b)/q'(0)$. At time $t_D = (b-a)/\left(\frac{q(\overline{\rho})}{\overline{\rho}} - q'(\overline{\rho})\right)$, the shock and the rarefaction in (1.8) start to interact, yielding the shock S_1, see Figure 1.15. Due to the interaction, S_1 accelerates and the state to its right decreases. If $\overline{\rho} \leq \rho'_M$, then the outflow through the door is always less than the maximal one and panic does not arise. Therefore, assume that $\overline{\rho} \in]\rho'_M, R[$.Then, at time $t_E = (L-b)/q'(\rho'_M)$, the maximal outflow through the door is reached, provided not all people already exited, i.e. provided

$$(b-a)\overline{\rho} > \int_{t_c}^{t_E} q(\rho(t, L-))dt$$

which, in turn, is ensured if (1.7) holds. A backward shock with support S_2 is formed at E and it immediately starts to interact with the rarefaction exiting B and

accelerates backwards, so that it is bent as in Figure 1.15, right. Along the right side of S_2 the density is constantly equal to ρ''_M, while on its left side it increases. Therefore, the expression (1.9) yields a solution to (1.8) for $t \leq \min\{t_D, t_E\}$.

If S_1 hits S_2 before the state to the left of S_2 reaches the value s, then no panic arises and people exit the door exploiting its maximum outflow. On the other hand, if

$$\frac{b-a}{L-b} > \left(\frac{q(s)}{s} - q'(s)\right) \cdot \frac{\frac{q(\overline{\rho})}{\overline{\rho}} - q'(\overline{\rho})}{\frac{q(s)}{s} - q'(\overline{\rho})} \cdot \frac{q'(\rho''_M) - \frac{p_M - q(s)}{\rho''_M - s}}{q'(s) - \frac{p_M - q(s)}{\rho''_M - s}} \cdot \frac{1}{q'(\rho''_M)}, \tag{1.10}$$

then the state to the left of S_2 reaches the value s at F and the two shocks S_1, S_2 do not interact.

Then, by (1.6), $p_M < q(s + \Delta s)$, the jump across S_2 at F is greater than s. (**R1**) prescribes to solve the Riemann problem at F with a nonclassical shock $\mathcal{N}_1$ between s and $\psi(s)$, followed by a rarefaction and by a classical shock S_3 between the states $\psi(\rho''_M)$ and ρ''_M. By the assumption $p_M < q(R^*_M)$, the classical shock S_3 has positive speed. In other words, at time t_F, panic outbreaks at x_F and fills the region bounded between the nonclassical shock $\mathcal{N}_1$ and the classical shock S_3.

Note that condition (1.10) that has a key role in the outbreak of panic, has a clear geometric interpretation: it requires that the space initially occupied by the people be large with respect to the initial distance of the people from the door. They underline the geometric nature of (1.10). Indeed, due to (**Q**), the second factor in the right hand side of (1.10) is bounded above by 1, so that (1.10) can be substituted by the stronger condition

$$\frac{b-a}{L-b} > \left(\frac{q(s)}{s} - q'(s)\right) \cdot \frac{q'(\rho''_M) - \frac{p_M - q(s)}{\rho''_M - s}}{q'(s) - \frac{p_M - q(s)}{\rho''_M - s}} \cdot \frac{1}{q'(\rho''_M)},$$

which is independent from the (sufficiently large) initial density $\overline{\rho}$.

The nonclassical shock $\mathcal{N}_1$ hits the shock S_1 in a point, say H, leading to a nonclassical shock $\mathcal{N}_2$ between the left state 0 and a right state, that they assume varies in the interval $]\rho'_m, \rho''_m[$.

The nonclassical shock $\mathcal{N}_2$ may hit S_3 before it reaches $x = L$. In this case, the panicking crowd does not reach the door and the lower outflow p_m is not attained. On the other hand, if the total amount of people initially present $(b-a)\overline{\rho}$ is

sufficiently high, then the shock S_3 reaches the door at G and the outflow through the door falls to the lower value p_m. From G a classical shock curve S_4 arises between a state on its left varying in $]\rho'_m, \rho''_m[$ and ρ''_m on its right.

Finally, S_4 interacts with $\mathcal{N}_2$ giving rise to a nonclassical shock $\mathcal{N}_3$, between the states 0 and ρ''_m, that eventually gets to the door at I, t_I being the total time necessary to empty the corridor. In the time interval between t_G and t_I the door outflow is the lower value p_m, describing the fall in the door efficiency, typical of panicking situations.

1.3 The approach by Bellomo and Dogbé

The first step in modelling real systems is the identification of the observation and modelling scales. Subsequently, for each scale one has to identify the parameters and the variables to be used toward modelling. Classically, the following types of description can be considered:

Microscopic description: All pedestrians, regarded as particles, are individually identified. Position and velocity, regarded as dependent variables of time, of all individuals define the state of the whole system.

Kinetic description: The state of the system is identified by a suitable probability distribution over the microscopic state of the test individual representative of the whole system.

Macroscopic description: The state is described by locally averaged quantities, namely density, mass velocity and energy, regarded as dependent variables of time and space.

In details, let us consider a large system of individuals, regarded as active particles, over a two-dimensional domain $\Omega \in \mathbb{R}^2$, which may be either bounded or unbounded. The following parameters can be used toward the identification of dimensionless independent and dependent variables at the various scale:

- ℓ is a characteristic length of the system. If Ω is bounded, is the largest dimension; if Ω is unbounded, then is the largest dimension of the domain containing the initial localization of the crowd.

- n_M is the maximum density of the crowd corresponding to their admissible packing;

- V_M is the maximum admissible mean velocity of crowd which may be reached, in average, in free flow conditions, while the maximum admissible velocity for an isolated individual, may be larger that V_M is denoted by $(1+\mu)V_M, \mu > 0$.

The above quantities allow the assessment of the following independent variables:

- $t = t_r/T_C$, where t_r is the real time, is the dimensionless time variable referred to the critical time $T_C = V_M/\ell$.
- $x = x_r/\ell$, and $y = y_r/\ell$ which are the dimensionless space variables obtained referring to the real space variables x_r and y_r to ℓ.

The *microscopic representation* is defined by the following variables:

$x_i = \{x, y\}_i$, which identifies, for $i = 1, ..., N$, the position in Ω of each ith individual of a crowd of N individuals;

$V_i = \{V_x, V_y\}_i$, which identifies the dimensionless (being referred to V_M, velocity of each ith individual of the crowd.

Mathematical models are generally stated as a system of N ordinary differential equations where v_i and x_i are the dependent variables, that are normalized with respect to V_M and ℓ, respectively.

The *kinetic (statistical) representation* of a system constituted by a large number of interacting individuals is defined by the statistical distribution of their position and velocity:

$$f = f(t, x, V) = f(t, x, y, V_x, V_y),$$

where, if f is locally integrable, $f(t, x, V)dxdV$ denotes the number of individuals, which, at the time t, are in the elementary domain of the microscopic states $[x, x + dx] \times [y, y + dy] \times [V_x, V_x + dV_x] \times [V_y, V_y + dV_y]$.

The distribution function f can be normalized with respect to n_M, while also in this case the microscopic variables are normalized with respect to V_M and ℓ, respectively. Therefore, all derived variables can be given in a dimensionless form. Macroscopic observable quantities can be obtained, under suitable integrability assumptions, by moments of the distribution. In particular, the dimensionless local density is given by

$$\rho(t,x) = \int_0^{1+\mu} \int_0^{1+\mu} f(t,x,V)dV.$$

The total number of individuals in Ω, at time t, is given by

$$\rho(t,x) = \int_\Omega \rho(t,x)dx.$$

Analogously, the mean velocity can be computed as follows:

$$\overrightarrow{v}(t,x) = E[V](t,x) = \frac{1}{\rho(t,x)} \int_0^{1+\mu} \int_0^{1+\mu} V f(t,x,V)dV.$$

and similarly the speed variance

$$\sigma(t,x) = \frac{1}{\rho(t,x)} \int_0^{1+\mu} \int_0^{1+\mu} [V - E[V](t,x)]^2 f(t,x,V)dV.$$

where the speed variance provides a measure of the stochastic behavior of the system with respect to the deterministic macroscopic description. Mathematical models obtained, in the framework of the kinetic theory, by evolution equations for the above defined distribution function obtained by number density balance in the elementary volume of the space of the microscopic states. Inflows and outflows into and from such a volume are determined by interactions between the test individual and the field ones.

The mathematical kinetic theory for active particles suggests adding to the modelling of the microscopic state an additional activity variable suitable to describe the strategy of each individual regarded as an active particle.

The *macroscopic representation* of a system constituted by a large number of interacting individuals concerns groups of pedestrians rather than the individual units. Macroscopic representation may be selected for high density, large scale systems in which the local behavior of groups is sufficient.

$\rho = \rho(t,x,y)$ which is the dimensionless density referred the local number density;

$n = n(t,x,y)$ to the maximum admissible density n_M;

$\overrightarrow{\nu} = \overrightarrow{\nu}(t,x,y)$ that is the dimensionless mean velocity, referred to V_M, that, in two space dimensions, expressed by the unit vectors denoted by $(\overrightarrow{i}, \overrightarrow{j})$, writes:

$$\overrightarrow{\nu}(t,x,y) = v_x(t,x,y)\overrightarrow{i} + v_y(t,x,y)\overrightarrow{j}.$$

The relationship between the flow rate, the mean velocity and the pedestrian density is given, in dimensionless form, as follows: $\overrightarrow{q} = \rho\overrightarrow{\nu}$.

Classically, equation of conservation of mass and equilibrium of linear momentum can be used. The main conceptual difficulty consists in modelling the closure of momentum equation by suitable phenomenological models of the acceleration applied to individuals in the elementary volume $dx = dxdy$.

Pedestrian movement shows characteristics different from those of cars or other vehicles. Pedestrians have more flexibility to move in two dimensions, as well as more flexibility to stop and go within the full range of admissible velocities, that is not the case of vehicles. This is due to the wide domain of visibility area controlled by them. However, the hydrodynamic approach refers to locally averaged quantities, therefore local fluctuations in the velocity are not modelled explicitly.

Bearing all the above in mind, let us consider the modelling approach offered by continuum mechanics that approximates the system under consideration as a continuum flow. Therefore, if the distances between the crowds are assumed to be negligible. The state of the system, in two space dimensions, is described by density of the crowd and the average speed: $\rho = \rho(t, x, y)$ and $v = v(t, x, y)$, while the local flow is given by:

$$\overrightarrow{q} = \overrightarrow{q}(t, x, y) = \rho(t, v, y)\overrightarrow{\nu}(t, v, y),$$

where, according to the continuum approach, the above quantities are supposed to be differentiable with respect to the dependent variables.

Referring to figure 1.16, let us consider, the crowd in a bounded domain $\Omega \subset \mathbb{R}^2$, where $\partial\Omega$ is its boundary. The overall description of the system is delivered by the equation of conservation of mass and equilibrium of linear momentum defined by the following system of partial differential equations:

$$\begin{cases} \partial_t \rho + \nabla_x \cdot (\rho \overrightarrow{v}) = 0 \\ \partial_t \overrightarrow{v} + \overrightarrow{v}(\nabla_x \cdot \overrightarrow{v}) = \overrightarrow{F}[\rho, \overrightarrow{v}], \end{cases} \tag{1.11}$$

where F models the average acceleration that acts over the elementary block of individuals in volume $dxdy$. Here ∂t stands for the partial time derivative. The notation $(\cdot)\varphi = \frac{\partial(\cdot)}{\partial\varphi}$ will be used here after. The first equation being pedestrian conservation and the second speed dynamics; brackets are used to indicate that

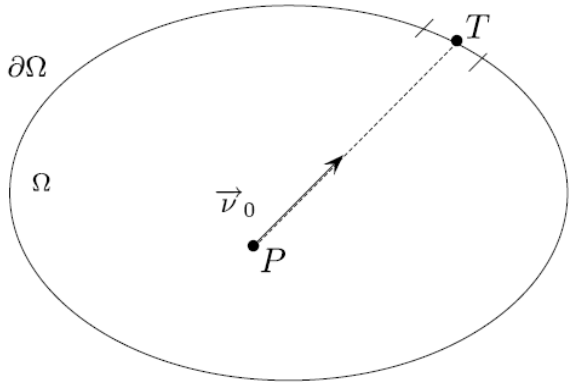

Figure 1.16: Geometry of the domain occupied by the crowd.

in equation 1.11, $\overrightarrow{F} = \{Fx, Fy\}$ can be, in specific models, a functional of its arguments, for instance it can be a function not only from ρ and $\overrightarrow{v}$ but also of their space derivative.

The above system acts as the general framework for the derivation of specific models which can be classified as first-order models if only the mass conservation equation is used and is properly closed by a phenomenological model linking the velocity to the local density conditions (including density gradients), while second-order models refer to the whole system and are obtained by closing the linear momentum equation by a phenomenological model of the term F.

$\overrightarrow{F}$ is not the real physical force applied by an external field; it characterizes the internal driving force or motivation of the pedestrian.

A preliminary observation, still waiting for the derivation of models, is that pedestrians have a target to reach, for instance a point T of the boundary corresponding to the exit. Therefore, given a point $P = \{x, y\}$ inside Ω is useful, for the calculations developed in the next section, defining the unit vector from P to the target T as shown in figure 1.11.

The calculation of the unit vector $\overrightarrow{v}_0$, according to the geometry of the system, is simply as follows:

$$\overrightarrow{\nu}_0(x, y) = \overrightarrow{\nu}_{x0}(x, y) + \overrightarrow{\nu}_{y0}(x, y),$$

where

$$\overrightarrow{\nu}_{x0}(x,y) = \frac{x - x_T}{\sqrt{(x-x_T)^2 + (y-y_T)^2}}\overrightarrow{i},$$

and

$$\overrightarrow{\nu}_{y0}(x,y) = \frac{y - y_T}{\sqrt{(x-x_T)^2 + (y-y_T)^2}}\overrightarrow{j},$$

where the direction of the vector is simply identified by the coordinates of the points P and T.

Of ctheirse, pedestrians may have a target inside the domain Ω, simple technical modifications are needed to consider this case. The statement of mathematical problems needs suitable boundary conditions unless the modelling refers to crowds in unbounded domains. However, it is still reasonable for the crowd to have a target.

There are other models called *second-order models*, namely models with accelerations. All models consist of two equations given in a 2D system of partial differential equations (1.11) with a phenomenological relation that describes the average 2D acceleration by which the crowd modifies its own speed: $\overrightarrow{F} = \{F_x, F_y\}$, where the components of $\overrightarrow{F}$ may depend on the local density, density gradients, velocity and position of the crowd: $\overrightarrow{F} = \overrightarrow{F}[\rho, \overrightarrow{v}, \nu]$, where square brackets denote functional dependence.

Second-Order Models

Different classes of models can be identified according to different ways of modelling the aforementioned acceleration. Specifically, three classes of models here are considered simply identified by the way pedestrian select their direction of motion.

In details:

Class I: The first class refers to systems where the pedestrians move along straight lines toward the target objective.

Class II: The second class of models refers to walkers that still move toward the target objective, but are also attracted by paths with small density gradients.

Class III: The third class of models contains a "pressure" term which enables the momentum equation to predict the expect response of crowd behavior as time and space changes.

The above classification simply takes into account the direction followed by pedestrians, while different expression of the acceleration along such a direction can be proposed, as they shall see, according to their specific phenomenological behaviors.

The modelling is proposed in normal flow conditions. The dynamics in panic conditions is analyzed in the last section. The presentation of the various models follows the same guidelines: the fundamental assumptions that generate each class of models is stated, subsequently the mathematical framework is derived, and finally same specific models are derived based on suitable phenomenological assumptions concerning the acceleration term.

Class I Pedestrians seek to minimize their (accurately) estimated travel time but temper their velocity according to local density. Specifically, in each point $P = \{x_P, y_P\}$ of the domain, individuals move toward a given objective along the direction $\overrightarrow{\nu}_0(x, y)$. Moreover, their acceleration consists of two contributions: the first one corresponding to a trend and to equilibrium velocity depending on the local density, directed toward $\overrightarrow{\nu}_0(x, y)$, and the second term to the action of the density gradients toward $\overrightarrow{\nu}_0$. In particular, negative values increase the acceleration, while positive values decrease it.

The formal structure of the system corresponding to mass conservation and linear momentum equilibrium is as follows:

$$\begin{cases} \partial_t \rho + \partial_x(\rho v_x) + \partial_y(\rho v_y) = 0 \\ \partial_t v_x + v_x \partial_x v_x + v_y \partial_y v_x = F_{1x}(x, \rho, \overrightarrow{v}) + F_{2x}(x, \rho, \Delta\nu_0\rho) \\ \partial_t v_y + v_x \partial_x v_y + v_y \partial_y v_y = F_{1y}(x, \rho, \overrightarrow{v}) + F_{2y}(x, \rho, \Delta\nu_0\rho) \end{cases} \tag{1.12}$$

where the first term corresponds to the adaptation to the velocity $\overrightarrow{v}_e$, which depends on the local density, while the second term corresponds to the influence of local density gradients. The above acceleration terms can be specialized as follows:

$$\overrightarrow{F}_1 = \alpha(v_e(\rho)\overrightarrow{\nu}_0 - \overrightarrow{v}), \tag{1.13}$$

where α is a constant representing the inverse of the relaxation time of $\overrightarrow{v}$ toward the generalized equilibrium velocity $v(\rho)\overrightarrow{\nu}_0$ and

$$\overrightarrow{F}_2 = -\frac{K^2(\rho)}{\rho}\nabla_{\nu_0}\rho. \tag{1.14}$$

Inserting the above formal expression into (1.12) generates the following vector system:

$$\begin{cases} \partial_t\rho + \nabla_x \cdot (\rho\overrightarrow{v}) = 0, \\ \partial_t\overrightarrow{v} + (\overrightarrow{v}\cdot\nabla_x)\overrightarrow{v} = \alpha(v_e(\rho)\overrightarrow{\nu}_0 - \overrightarrow{v}) - \frac{K^2(\rho)}{\rho}\nabla_{\nu_0}\rho. \end{cases} \tag{1.15}$$

Different specific models can be derived in agreement with (1.15) according to different specific models (1.13) and (1.14). In particular, various models have been proposed in the mathematical literature for vehicular traffic flow to describe the trend defined in (1.13). The simplest model is based on the assumption of a linear decay: $v_e(\rho) = 1 - \rho$. However, this extremely simple model does not take properly into account as the quality of the environment, as the decay with respect to density depends on its quality. It may be less steepest when the quality of the environment is good. Various models can be derived by using different expressions of $K^2(\rho)$.

The above class of models can be further refined by taking the gradients along the local mean velocity. It is however a technical difference that does not introduce significant additional improvements.

Class II The class of models above described is such that pedestrians direct their motion, from any point P of the domain Ω, to the target T . On the other hand, the direction of motion generally takes into account the fact that pedestrians attempt to avoid zones with higher density, while the selection of optimal paths occurs only in their visibility zone. The reasoning has some analogy with that used in the modelling of pedestrian flow by first-order models. Conservation equations (1.12) or (1.15) are still used however the direction identified by the unit vector ν_0 must be substituted by a new one that takes into account the above phenomena. Specifically the following assumption is proposed:

Pedestrians seek to join the objective by undervalying their time if possible and at the same time while seeking to avoid the zones with high density. Pedestrians

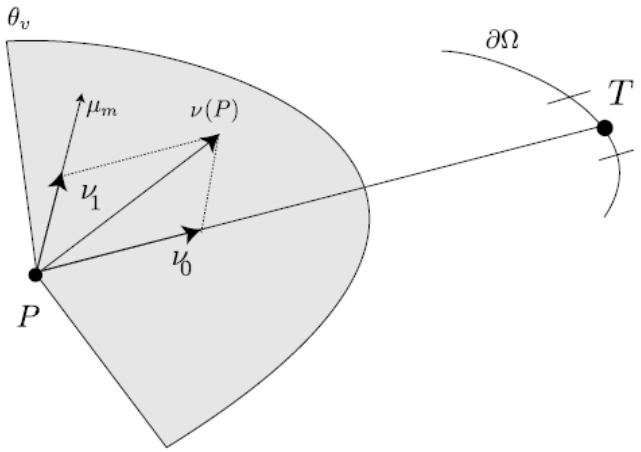

Figure 1.17: Target and visibility zone.

do not have a global vision of the situation, but their perception of the density is limited visual field.

The formalization of the above assumption into mathematical terms needs the identification of the *path-direction* ν and of the visibility zone, bearing in mind that the above two quantities are technically related. Bearing all above in mind let us define by

$$\gamma = \arctan\left(\frac{\nu_{0y}}{\nu_{0x}}\right)$$

the angle which characterizes the direction of the vector ν_0, and by Θ_ν the maximum angle of visibility of the pedestrian (in average), one can define a "visual range" interval:

$$R_v = [\gamma - \Theta_\nu, \gamma + \Theta_\nu]$$

to the inside of which the direction toward which heading is chosen. Therefore, let us define the following quantity

$$I = \left[\overrightarrow{\xi}\cos\alpha\,\overrightarrow{i} + \sin\alpha\,\overrightarrow{i}\,|\alpha \in R_v\right]$$

and by $\overrightarrow{\mu}_m = \overrightarrow{\mu}_m(P)$ the minimal direction of the directional derivative

$$\min_{\overrightarrow{\xi} \in I} \left[\nabla_x \rho(P) \cdot \overrightarrow{\xi} \right]$$

where I is the domain of the path directions on R_v.

The direction of the motion of pedestrians can be defined, given a density field, as follows:

$$\overrightarrow{\nu}(P) = \overrightarrow{\nu}_0(P) + \overrightarrow{\nu}_1(P), \tag{1.16}$$

where the corrective term is given by

$$\overrightarrow{\nu_1}(P) = \eta \overrightarrow{\mu}_m(P) \tag{1.17}$$

where η is a positive small parameter introduced to model a corrective term related to the attraction toward small density gradients.

Mathematical models are then related to the following structure:

$$\begin{cases} \partial_t \rho + \nabla_x \cdot (\rho \overrightarrow{v}) = 0, \\ \partial_t \overrightarrow{v} + (\overrightarrow{v} \cdot \nabla_x) \overrightarrow{v} = \overrightarrow{F}[\rho, \overrightarrow{v}] = \alpha(v_e(\rho) \overrightarrow{\nu} - \overrightarrow{v}) - \frac{K^2(\rho)}{\rho} \nabla_{\overrightarrow{\nu}} \rho. \end{cases}$$

that uses, with respect to (1.16), the direction ν instead of ν_0. Specific models are obtained by adopting suitable expressions of the terms ve and $K^2(\rho)$. Although technically more complex, the above modelling method has the advantage of leading to an immediate modelling approach of panic conditions. It is worth stressing that further developments can be obtained by taking into account additional phenomena in the modelling of the acceleration term $\overrightarrow{F}[\rho, \overrightarrow{v}]$ for instance, a linear velocity diffusion term corresponding to a viscous dissipation in fluid dynamical framework can be added. Consequently, the acceleration of pedestrians will be given by three contributions: the first corresponds to a trend to equilibrium, the second to the action of the density gradient and the third to a dissipative velocity diffusion

$$\overrightarrow{F}[\rho, \overrightarrow{v}] = \overrightarrow{F_1}[\rho, \overrightarrow{v}] + \overrightarrow{F_2}[\rho, \overrightarrow{v}] + \overrightarrow{F_3}[\rho, \overrightarrow{v}] = c_1(\overrightarrow{v}_e - \overrightarrow{v}) - \frac{1}{\rho} \nabla_x p + \frac{\epsilon}{\rho} \Delta \overrightarrow{v}$$

where ϵ is a parameter positive which represents in the case of the fluids, the viscosity.

Class III The various models proposed have been obtained by using conservation of mass and linear momentum. The analysis of traffic flow modelling has shown that it can be useful a modelling approach based on the conservation of different quantities such as the total pressure. their model of Class III is based on a 1D traffic flow model proposed by Aw and Rascle [1].

The first equation is the two-dimensional conservation law equation given by

$$\partial_t \rho + \partial_x(\rho v_x) + \partial_y(\rho v_y) = 0.$$

The second equation is obtained by applying the convective derivative on the pressure terms for the 2D case and it is given by

$$\begin{gathered}\partial_t(v_x + P_1(\rho, v_x)\overrightarrow{\nu_0}) + v_x\partial_x(v_x + P_1(\rho, v_x)\nu_{x_0}) + \\ v_y\partial_y(v_x + P_1(\rho, v_x)\nu_{x_0}) = \rho\mathcal{A}_1\left[\rho, \overrightarrow{v}\right], \\ \partial_t(v_x + P_2(\rho, v_x)\overrightarrow{\nu_0}) + v_x\partial_x(v_x + P_2(\rho, v_x)\nu_{x_0}) + \\ v_y\partial_y(v_x + P_2(\rho, v_x)\nu_{x_0}) = \rho\mathcal{A}_2\left[\rho, \overrightarrow{v}\right],\end{gathered}$$

where $P(\rho, \overrightarrow{v})$ is a proposed function given by

$$P(\rho, \overrightarrow{v}) = \frac{\rho^{\gamma+1}}{\beta - \rho^{\gamma+1}}\overrightarrow{v}$$

and valid for $\gamma > 0$ is a dimensionless constant and $\beta > \rho_m^{\gamma+1}$ with ρ_m means the maximum density and

$$\begin{aligned}\mathcal{A}_1\left[\rho, \overrightarrow{v}\right] &= \alpha(v_e(\rho)\nu_{x_0} - v_x); \\ \mathcal{A}_2\left[\rho, \overrightarrow{v}\right] &= \alpha(v_e(\rho)\nu_{y_0} - v_y).\end{aligned}$$

In a more compact form, the system of Class III can be written as follows:

$$\begin{cases} \partial_t \rho + \nabla_x \cdot (\rho\overrightarrow{v}) = 0, \\ \partial_t(\overrightarrow{v} + P(\rho, \overrightarrow{v})\overrightarrow{\nu}_0) + (\overrightarrow{v \cdot \nabla_x}) + (\overrightarrow{v} + P(\rho, \overrightarrow{v})\overrightarrow{\nu}_0) = \mathcal{A}_1\left[\rho, \overrightarrow{v}\right], \end{cases} \tag{1.18}$$

while, in dimensionless variables, equation (1.18) is as follows:

$$\begin{cases} \partial_t \rho + \rho(\partial_x v_x + \partial_y v_y) + \rho \partial_x v_x + \rho \partial_y v_y = 0, \\ \partial_t (v_x + P_1(\rho, v_x)\nu_{x_0}) + v_x \partial_x (v_x + P_1(\rho, v_x)\nu_{x_0}) + \\ \qquad v_y \partial_y (v_x + P_1(\rho, v_x)\nu_{x_0}) = \rho \mathcal{A}_1 \left[\rho, \overrightarrow{v}\right], \\ \partial_t (v_x + P_2(\rho, v_x)\nu_{y_0}) + v_x \partial_x (v_x + P_2(\rho, v_x)\nu_{x_0}) + \\ \qquad v_y \partial_y (v_x + P_2(\rho, v_x)\nu_{x_0}) = \rho \mathcal{A}_2 \left[\rho, \overrightarrow{v}\right], \end{cases}$$

supplemented by initial conditions $\rho(0, x, y) \geq 0$, $v_x(0, x) \leq |v_{1x}|$ and $v_y(0, y) \leq |v_{2y}|$. Here v_{1x} and v_{2y} are the free flow speed.

An additional alternative is obtained by using for the first equation the twodimensional conservation of continuity that conserve mass (pedestrians) given by

$$\partial_t \rho + \partial_x(\rho v_x) + \partial_y(\rho v_y) = 0.$$

The flux flow rate in both directions is represented by ρv_x and ρv_y. The second equation is similar to the momentum equations in 2D for compressible flow with some manipulations to mimic crowd dynamics and it is given by

$$\begin{aligned} \partial_t v_x + v_x \partial_x v_x + v_y \partial_y v_y + \rho v_e'(\rho)\nu_{x_0}[\partial_x v_x + \partial_y v_y] &= \rho \mathcal{A}_1 \left[\rho, \overrightarrow{v}\right], \\ \partial_t v_y + v_x \partial_x v_x + v_y \partial_y v_y + \rho v_e'(\rho)\nu_{y_0}[\partial_x v_x + \partial_y v_y] &= \rho \mathcal{A}_2 \left[\rho, \overrightarrow{v}\right], \end{aligned}$$

where $\rho v_e'(\rho)$ and $\rho v_e'(\rho)$ are the traffic sound speed at which small traffic disturbances are propagated relative to the moving crowd stream. This model will be classified as a crowd flow nonlinear, time varying, hyperbolic system of two partial differential equations.

1.4 A macroscopic approach by Maury and Venel

Maury and Venel proposed to integrate a strong non-overlapping constraint in a ODE framework, in the spirit of granular flow models. Their approach rests on two principles. On the one hand, they define a spontaneous velocity, which corresponds to the velocity each individual would like to have in the absence of other people. On the other hand, individuals (which are identified to rigid discs) must obey a non-overlapping constraint. Those two principles lead us to define the actual velocity field as the projection of the spontaneous velocity over the set

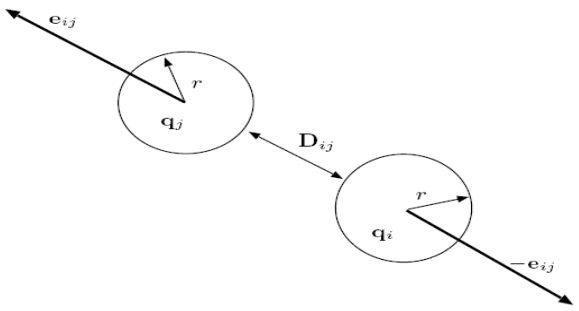

Figure 1.18: Notations

of admissible velocities (regarding the nonoverlapping constraints). To perform this projection, they put the problem in a saddle-point form, which leads us to introduce a collection of Lagrange multipliers. Those Lagrange multipliers can be interpreted as interaction pressure between people which are in contact.

Consider N persons identified with rigid disks of common radius r, in a room represented by a domain $\Omega \in \mathbb{R}^2$. The centre of the i-th disk is denoted by q_i. They define the set of configurations:

$$Q = \left\{ q = (q_1, q_2, ..., q_N) \in \mathbb{R}^{2N} \right\}.$$

Moreover, introduce a spontaneous velocity field

$$U = (U_1, U_2, ..., U_N),$$

where U_i represents the velocity which person i would like to have if he is alone. As a first step, the simplest model one may think of: all individuals have the same behavitheir, and they do not elaborate complex strategies to escape. Therefore introduce a global spontaneous velocity field $x \to U_0(x)$, and write

$$U(q) = (U_0(q_1), ..., U_0(q_N)).$$

In this hard-sphere approach, overlapping is strictly forbidden, which leads to the following set of feasible configurations:

$$Q_0 = \{ q \in Q, D_{ij}(q) = |q_i - q_j| - 2r \geq 0 \quad \forall i \neq j \}.$$

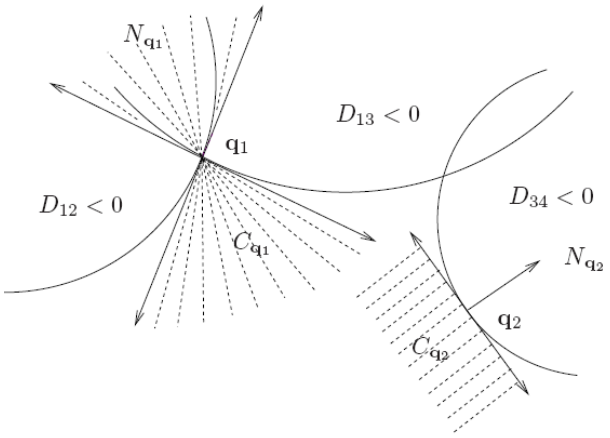

Figure 1.19: Cones $\mathcal{N}_q$ and $\mathcal{C}_q$

As overlapping is forbidden, two persons already in contact can only increase their distance: the set of feasible velocities is

$$\mathcal{C}_q = \{v, G_{ij}(q) \cdot v \geq 0 \text{ as soon as } D_{ij}(q) = 0\},$$

with (see Figure 1.18)

$$G_{ij} = \nabla D_{ij} = (0, ..., 0, -\mathbf{e}_{ij}, 0, ..., 0) \in \mathbb{R}^{2N}.$$

The basic form of the model: the actual velocity field is the feasible field which is the closest to U for the euclidean distance, which writes

$$\frac{dq}{qt} = P_{\mathcal{C}_q} U(q)$$

where $P_{\mathcal{C}_q}$denotes the euclidean projection onto the closed convex cone $\mathcal{C}_q$.

Despite its formal simplicity, this model does not fit directly into a standard framework. Let us reformulate the problem by introducing $\mathcal{N}_q$, the outward normal cone to the set of feasible configurations Q_0

$$\mathcal{N}_q = \mathcal{C}_q^0 = \{w, (w, v) \leq 0 \ \ \forall v \in \mathcal{C}_q\}.$$

Thanks to Farkas' Lemma, this cone can be expressed

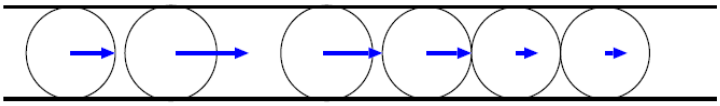

Figure 1.20: One dimensional situation

$$\mathcal{N}_q = \left\{ -\sum \lambda_{ij} G_{ij}, \lambda_{ij} \geq 0, D_{ij}(q) = 0 \Longrightarrow \lambda_{ij} = 0 \right\}.$$

Now using the classical orthogonal decomposition of a Hilbert space as the sum of mutually polar cone (see [29]), they obtain

$$\frac{dq}{qt} = P_{\mathcal{C}_q} U(q) = U(q) - P_{\mathcal{N}_q} U(q).$$

As a consequence,

$$\frac{dq}{qt} + \mathcal{N}_q \ni U(q). \tag{1.19}$$

The problem takes the form of a differential inclusion, which has motivated a huge amount of papers in the last decades. Let us first consider a special situation where standard theory can be applied. Consider N individuals in a corridor (see Figure 1.20). In that case, as people are not likely to leap accross each

other, it is natural to restrict the set of feasible configurations to one of its connected components:

$$Q_0 = \{ q = (q_1, q_2, ..., q_N), q_{i+1} \geq 2r \}.$$

In this very situation, as Q_0 is closed and convex, the multivalued operator $q \rightarrow \mathcal{N}_q$ identifies to the subdifferential of the indicatrix function of Q_0:

$$\partial I_{Q_0}(q) = \{ v, I_{Q_0}(q) + (v, h) \leq I_{Q_0}(q+h) \quad \forall h \}, \; I_{Q_0}(q) = \left| \begin{array}{ll} 0 & \text{if } \; q \in Q_0 \\ +\infty & \text{if } q \notin Q_0 \end{array} \right.$$

therefore $q \rightarrow \mathcal{N}_q$ is maximal monotone. As soon as the spontaneous velocity is regular (i.e. Lipschitz), standard theory (see e.g. [7]) ensures wellposedness. In the general case, Q_0 is not convex, so that $q \rightarrow \mathcal{N}_q$ is not maximal monotone. Despite

the formal simplicity of the model, its analysis calls for sophisticated abstract tools developped recently by Edmond and Thibault [18]. The well-posedness rests on the fact that the set of feasible configurations is prox-regular (see [12]) , which means that the projection onto Q_0 is well-defined in its neighbtheirhood. As a consequence, it can be established that the problem is well-posed.

The numerical scheme proposed by Maury and Venel is based on a first order expansion of the constraints expressed in terms of velocities. Introduce a uniform sequence of time steps

$$t^0 = 0 < t^1 < ... < t^p = T, \quad t^{n+1} - t^n = T/p,$$

and they denote by q^n the approximation of $q(t^n)$. The next configuration is obtained as

$$q^{n+1} = q^n + hu^{n+1},$$

where u^{n+1} minimizes

$$\frac{1}{2}\left|v - U(q^n)\right|^2 \text{ over } \mathcal{C}^h_{q^n}, \quad \text{with}$$

$$\mathcal{C}^h_q = \left\{v, D_{ij}(q) + hG_{ij}(q) \cdot v \geq 0\right\}.$$

In other words,

$$u^{n+1} = P_{\mathcal{C}^h_{q^n}}(U(q^n)).$$

This scheme can be shown to converge to the exact solution:

Theorem 1 *Let us denote by q_h the continuous, piecewise linear function associated to the numerical scheme. Then q_h goes to q uniformly in $[0, T]$, where $t \to q(t)$ is the exact solution.*

The scheme can be interpreted in the following way. Let us introduce the set

$$Q^h_0(q) = \left\{\tilde{q}, D_{ij}(q) + G_{ij}(q) \cdot (\tilde{q} - q \geq 0)\right\}.$$

which can be seen as an inner convex approximation of Q_0. Note that Q_0^h does not depend on h. Yet they keep this notation to emphasize the fact that it is an approximation of Q_0. It is straightforward to check that

$$\frac{q^{n+1}-q^n}{h} + \partial I_{Q_0^h(q^n)}(q^{n+1}) \ni U(q^n)$$

so that the scheme can be seen as a semi-implicit discretization of (1.19), where $\partial I_{Q_0^h(q^n)}$ approximates $\mathcal{N}_{q^n}$.

The costly part of the algorithm lies in the projection of the spontaneous velocity onto the approximated set of feasible velocities. This projection can be solved by a Uzawa algorithm (note that any algorithm could be used to perform this task). This algorithm (see e.g. [9]) is based on a reformulation of the projection problem onto a saddle-point form:

$$\begin{cases} u + B^*\lambda = U \\ Bu \leq D \\ (Bu - D, \lambda = 0) \end{cases}$$

with

$$\begin{aligned} U &= U(q^n), Bv = (-hG_{ij}(q^n)\cdot v)_{i<j}, D = (D_{ij}(q^n))_{i<j}, \\ B^*\lambda &= -h\sum_{i<j}\lambda_{ij}G_{ij}(q^n). \end{aligned}$$

The Uzawa algorithm produces a sequence λ^k according to

$$\lambda^{k+1} = \Pi_+(\lambda^k + \rho(B(U - B^*\lambda^k) - D)),$$

where Π_+ is the euclidean projection onto the cone of vectors with nonnegative components (a simple cut-off in practice), and $\rho > 0$ is a fixed parameter. The algorithm can be shown to converge as soon as $0 < \rho < 2/\|B\|^2$ (see [29]).

Experiments The first set of experiments is based on the following situation: consider two populations of individuals in a periodic bidimensional domain. They are represented in black (B) and white (W) in the figures. B-individuals want to go to the right, and W-individuals tend to go in the opposite direction (with the same

desired speed 1). The simplest model proposed, without any avoiding strategies, makes it possible to recover the so-called fingering pattern (see [20], [22]). The number of inviduals in each population is 750. Figure 1.21 represents snapshots of the two populations, at times 0 (random distribution), 25, 75, and 100. Note on the second figure from the top, during the transitory period, the apparition of white and black clusters, due to absence of any social force or auto-optimization strategy in this test.

The second performed experiment corresponds to the situation of 3000 persons which are randomly distributed in a room at initial time. The spontaneous velocity field has constant modulus 1, and is directed along streamlines of the geodesic distance to a safe spot, far away from the room. The current configuration and the corresponding network of interaction pressures: for any couple of discs in contact, the segment between centers, having its color (from white to black) depend upon the (positive) Lagrange multiplier which handles the corresponding contraint is represented.

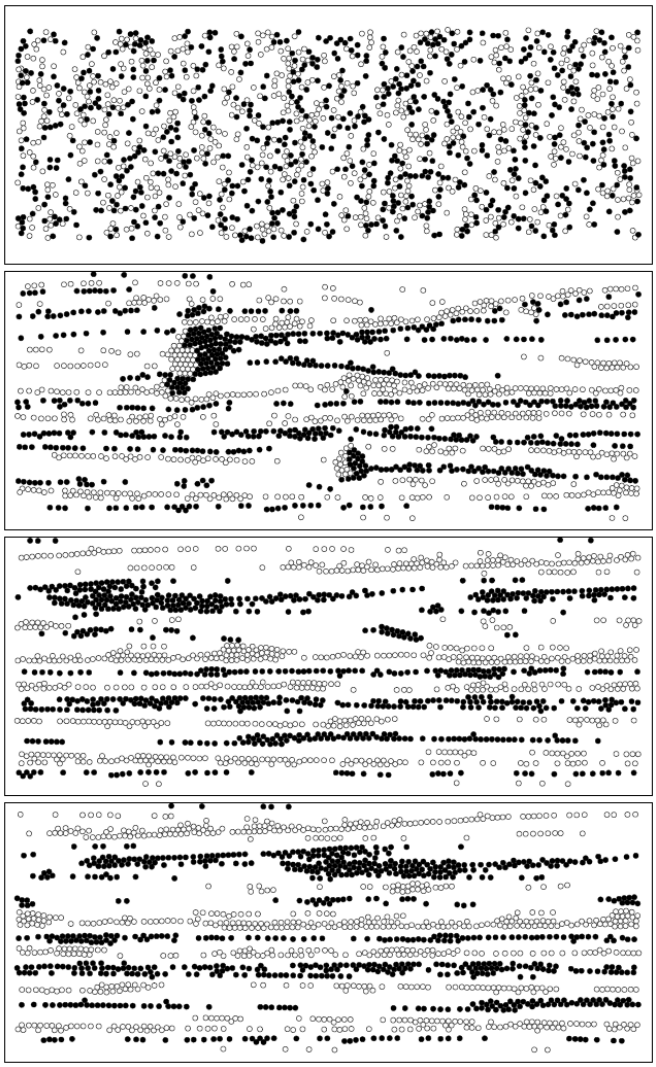

Figure 1.21: Counter flowing crowds

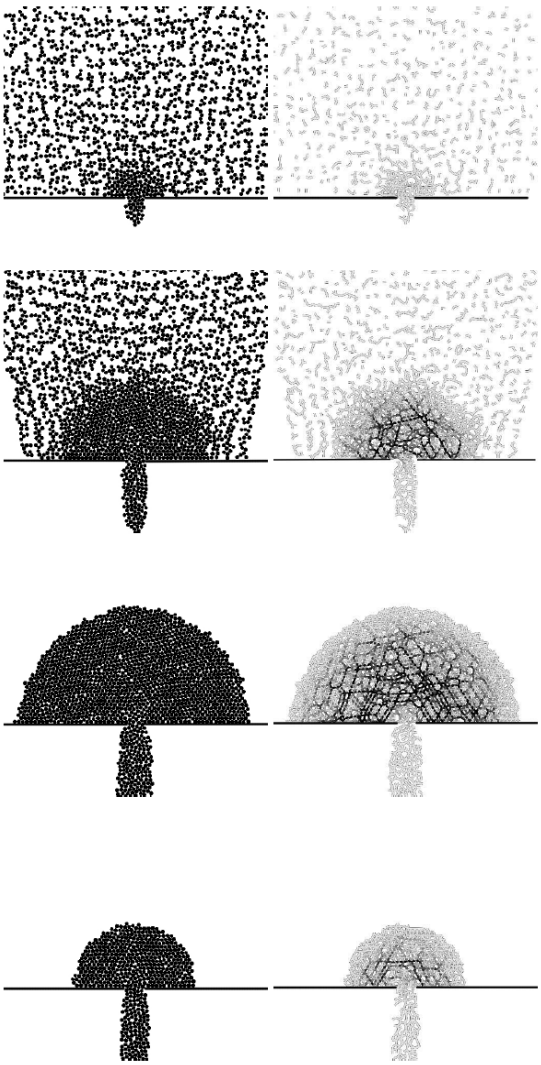

Figure 1.22: Emergency exit

Chapter 2

The model

In the model proposed by Piccoli, Benedetti and Tosin, microscopic and macroscopic scales coexist and continuously share information on the overall dynamics. More precisely, the microscopic part tracks the trajectories of single pedestrians and the macroscopic part the density of pedestrians using the same evolution equation duly interpreted in the sense of measures. In this respect, the two scales are indivisible. This makes the difference from other ways of understanding multiscale approaches in the literature.

From the mathematical point of view the mass of a d-dimensional system ($d = 1, 2, 3$ for physical purposes) at time t is a Radon positive measure μ_t that we assume to be defined on the Borel α-algebra $\mathcal{B}(\mathbb{R}^d)$. For any $E \in \mathcal{B}(\mathbb{R}^d)$ the mass of pedestrians contained in E at time $t \geq 0$ is given by the number $\mu_t(E) \geq 0$. In principle, the only further property satisfied by μ_t is the α-additivity, directly translating the principle of additivity of the mass.

Let $T > 0$ denote a certain final time. Following [8], the velocity field $v = v(t, x)$: $[0, T] \times \mathbb{R}^d \to \mathbb{R}^d$ transports a mass and the equation

$$\frac{\partial \mu_t}{\partial t} + \nabla \cdot (\mu_t v) = 0, \qquad (t, x) \in (0, T] \times \mathbb{R}^d \tag{2.1}$$

expresses the conservation of this mass along with some given initial distribution of mass μ_t (initial condition). Derivatives appearing in (2.1) are meant in the functional sense of measures. Specifically, for every smooth test function Φ with compact support (i.e., $\Phi \in C_c^\infty(\mathbb{R}^d)$), and for a.e. $t \in [0, T]$, it results

$$\frac{d}{dt}\int_{\mathbb{R}^d}\Phi(x)d\mu_t(x) = \int_{\mathbb{R}^d} v(t,x)\cdot\nabla\Phi(x)d\mu_t(x), \tag{2.2}$$

where integration-by-parts has been used at the right-hand side. A sufficient condition for (2.2) to be well-defined is that $v(t,\cdot)$ is integrable w.r.t. μ_t for a.e. $t \in [0,T]$.

A family of time-evolving measures $\{\mu_t\}$, $t > 0$ is said to be a (weak) solution to (2.1) if, for all $\Phi \in C_c^\infty(\mathbb{R}^d)$, the mapping $t \to \int_{\mathbb{R}^d}\Phi(x)d\mu_t(x)$ is absolutely continuous and satisfies (2.2). In particular, the latter statement means

$$\int_{\mathbb{R}^d}\Phi(x)d\mu_{t_2}(x) - \int_{\mathbb{R}^d}\Phi(x)d\mu_{t_1}(x) = \int_{t_1}^{t_2}\int_{\mathbb{R}^d} v(t,x)\cdot\nabla\Phi(x)d\mu_t(x)dt, \tag{2.3}$$

for all $t_1, t_2 \in [0,T]$, $t_1 \leq t_2$, and all $\Phi \in C_c^\infty(\mathbb{R}^d)$.

2.1 Modeling the interactions among pedestrians

Equation (2.1) provides the evolution of the measure μ_t as long as the velocity is specified. In our case, given the absence of a balance of linear momentum, this implies modeling directly the field v. For this reason, the approach will result in a first order model.

First order models are quite common in the literature, especially at the macroscopic scale. The velocity can be either specified as a known function ([12]) or linked to the density ρ of pedestrians by means of empirical fundamental relations $v = v(\rho)$ ([24], [10], [32]). Sometimes a functional dependence on the density gradient is envisaged, in order to model the sensitivity of pedestrians to the variations of the surrounding density field ([9], [13]). Microscopic models focus instead more closely on the interactions among pedestrians, normally expressing them in terms of generalized forces. They resort therefore to a classical Newtonian paradigm, in which the acceleration is modeled explicitly ([23], [20]). We remark, however, that in ([25], [27]) the authors adopt a kinematic modeling of the interactions in the frame of a microscopic model.

With the aim of setting up a model based on the mass conservation only, but in which the microscopic granularity complements the macroscopic dynamics, we cannot entirely resort either to generalized forces or to fundamental relations. Taking advantage of the mass conservation equation in the form (2.2), which does not assume a priori any modeling scale, our approach will be at the same time kinematic, macroscopic, and focused on the strategy developed by pedestrians at the microscopic scale.

To be more specific, let the velocity be expressed in the following form:

$$v(t,x) := v[\mu_t](x) = v_{des}(x) + \nu[\mu_t](x), \tag{2.4}$$

the square brackets denoting functional dependence on the measure μ_t.

The function $v_{des} : \mathbb{R}^d \to \mathbb{R}^d$ is the desired velocity that is the velocity a pedestrian would have in the absence of other surrounding pedestrians. This component of the total velocity describes the preferred direction of motion toward specific targets, possibly taking into account the presence of intermediate obstacles within the domain. Therefore, it is not affected by the actual crowding of the environments, but it specifically depends on the geometry of the walking area (in this sense, it is a sort of field velocity).

It is not restrictive to assume that it has constant modulus

$$|v_{des}(x)| = V, \quad \forall x \in \mathbb{R}^d, \tag{2.5}$$

where V represents some characteristic speed of the walkers. We refer the reader to [30] for a possible method to construct v_{des}.

The function $v[\mu_t] : \mathbb{R}^d \to \mathbb{R}^d$ is the interaction velocity that expresses the deviation of pedestrians from their preferred path due to the presence of other surrounding pedestrians. The nonlocality of the interactions is introduced in this framework by deriving $v[\mu_t]$ from a synthesis of the information on the crowd distribution around each pedestrian. Specifically, we assume

$$v[\mu_t](x) = \int_{\mathbb{R}^d/\{x\}} f(|y-x|)g(\alpha_{xy})\frac{y-x}{|y-x|}d\mu_t(y), \tag{2.6}$$

where

- $f : \mathbb{R}_+ \to \mathbb{R}$ is a function with compact support describing how the walker in x interacts with her neighbors on the basis of their distance. If supp $f = [0, R]$ for some $R > 0$, then a neighborhood of interaction is defined for the point x coinciding with the ball $B_R(x) \subset \mathbb{R}^d$ centered in x with radius R;

- $\alpha_{xy} \in [-\pi, \pi]$ is the angle between the vectors $y - x$ and $v_{des}(x)$, that is, the angle under which a point y is seen from x w.r.t. the desired direction of motion;

- $g : [-\pi, \pi] \to [0, 1]$ is a function which reproduces the angular focus of the walker in x.

Integration w.r.t. μ_t accounts for the mass that the walkers see, considering that two fundamental attitudes characterize pedestrian behavior:

- repulsion, i.e., the tendency to avoid collisions and crowded areas,

- attraction, i.e., the tendency, under some circumstances, to not lose the contact with other group mates (e.g., groups of tourists in guided tours, groups of people sharing specific relationships such as families or parties).

Focusing on one of the simplest choices, nonetheless physiologically sound, we suggest for f the following expression:

$$f(s) = -\frac{F_r}{s}\chi[0, R_r](s) + F_a s \chi[0, R_a](s), \tag{2.7}$$

where $F_r, F_a > 0$ are repulsion and attraction strengths, and $R_r, R_a > 0$ are repulsion and attraction radii. This form of f translates the basic idea that repulsion and attraction are inversely and directly proportional, respectively, to the distance separating the interacting pedestrians.

Interactions can be either metric or topological. An interaction is metric if the corresponding radius is fixed, so that each walker interacts with all other pedestrians within that given maximum distance. Conversely, an interaction is topological if the corresponding radius is adjusted dynamically by each walker, in such a way that the neighborhood of interaction encompasses a predefined mass of other pedestrians she feels comfortable to interact with. Here we will be mainly concerned

with metric interactions, for both repulsion and attraction. The interested reader is referred to ([2], [15]), and references therein, for a detailed discussion of metric and topological effects, also by means of examples and numerical simulations.

The function g carries the anisotropy of the interactions, which essentially consists in that pedestrians cannot see all around them and they are not equally sensitive to external stimuli coming from different directions. If $\overline{\alpha} \in [0, \pi]$ is the maximum sensitivity angular width, a very simple form of g is

$$g(s) = [-\overline{\alpha}, \overline{\alpha}](s), \ \ s \in [-\pi, \pi]. \tag{2.8}$$

By mollifying this function it is possible to account for the visual fading that usually occurs laterally in the visual field when approaching the maximum angular width.

2.2 The multiscale approach

In this section we first briefly review the methodology proposed in [15] to study microscopic and macroscopic self-organization in animal groups and crowds. Then, exploiting the tools offered by the measuretheoretic setting, we merge these concepts into a unique multiscale model, in which the microscopic and the macroscopic dynamics coexist.

2.2.1 Microscopic model

Let us consider $\{P_j(t)\}_{j=1}^N$ that denote the positions at time t of N pedestrians. In this case the mass of a set $E \in \mathcal{B}(\mathbb{R}^d)$ is the number of pedestrians contained in E; that is

$$\mu_t(E) = \operatorname{card}\{P_j(t) \in E\}, \tag{2.9}$$

hence μ_t is the counting measure. We represent it as a sum of Dirac masses, each centered in one of the P_j's

$$\mu_t = \sum_{j=1}^{N} \delta_{P_j(t).} \tag{2.10}$$

Plugging this in (2.2) gives

$$\frac{d}{dt}\sum_{j=1}^{N}\Phi\left(P_j(t)\right)=\sum_{j=1}^{N}v\left(t,P_j(t)\right)\cdot\nabla\Phi\in C_c^{\infty}(\mathbb{R}^d), \tag{2.11}$$

whence, taking the time derivative at the left-hand side and rearranging the terms,

$$\sum_{j=1}^{N}\left[\dot{P}_j(t)-v(t,P_j(t))\right]\cdot\nabla\Phi(P_j(t))=0, \tag{2.12}$$

the dot over P_j standing for derivative w.r.t. t. The arbitrariness of Φ implies

$$\dot{P}_j(t)=v[\mu_t](P_j(t)),\quad j=1,...,N, \tag{2.13}$$

where we have set $v\left(t,P_j(t)\right)=v[\mu_t](P_j(t))$ according to (2.4); therefore the microscopic model specializes in a dynamical system of N coupled ODEs for the P_j 's. The coupling is realized by the measure μ_t in the velocity field. In particular, the microscopic counterpart of (2.6) reads

$$v[\mu_t](P_j)=\sum_{\substack{k=1,...,N\\ P_k(t)\neq x}} f(|P_k-P_j|)g(\alpha_{kj})\frac{P_k-P_j}{|P_k-P_j|}, \tag{2.14}$$

where $\alpha_{kj}\in[-\pi,\pi]$ is shorthand for the angle formed by the vectors P_k-P_j and $v_{des}(P_j)$. We point out that, with the function f given by (2.7), the statement $P_k=P_j$ in the above formula can be converted into the milder one $k=j$. Indeed one can prove that if the P_j 's are initially all distinct they remain distinct at all successive times $t>0$ (see [16] for technical details).

2.2.2 Macroscopic models

Macroscopic models are based on the assumption that the matter is continuous, thus the measure μ_t is absolutely continuous w.r.t. the d-dimensional Lebesgue measure $\mathcal{L}^d$, $\mu_t\ll\mathcal{L}^d$. Radon–Nikodym's theorem asserts that there exists a function $\rho(t,\cdot)\in\mathcal{L}^1_{loc}(\mathbb{R}^d)$ such that

$$d\mu_t=\rho(t,\cdot)d\mathcal{L}^d,\quad \rho(t,\cdot)\geq 0 \text{ a.e.}, \tag{2.15}$$

called the density of μ_t w.r.t. $\mathcal{L}^d$. In our context $\rho(t,x)$ represents the density of pedestrians at time t in the point x.

Using ρ, the mass conservation equation (2.1) rewrites as

$$\frac{d}{dt}\int_{\mathbb{R}^d}\rho(t,x)\Phi(x)dx = \int_{\mathbb{R}^d}\rho(t,x)v(t,x)\cdot\nabla\Phi(x)dx, \quad \forall\Phi\in C_c^\infty(\mathbb{R}^d), \tag{2.16}$$

namely a weak form of the continuity equation

$$\frac{\partial\rho}{\partial t}+\nabla\cdot(\rho v)=0. \tag{2.17}$$

The interaction velocity specializes as

$$\nu[\mu_t](x)=\int_{\mathbb{R}^d}f(|y-x|)g(\alpha_{xy})\frac{y-x}{|y-x|}\rho(t,y)dy, \tag{2.18}$$

where it should be noticed that the domain of integration may now indifferently include or not the point x because $\{x\}$ is a Lebesgue-negligible set.

2.2.3 Multiscale models

If the measure μ_t is neither purely atomic nor entirely absolutely continuous w.r.t. $\mathcal{L}^d$ but includes both parts, we get models that incorporate the microscopic granularity of pedestrians in the macroscopic description of the crowd flow. More specifically, we consider

$$\mu_t=\theta m_t+(1-\theta)M_t, \tag{2.19}$$

where

$$m_t=\sum_{j=1}^{N}\delta_{P_j(t)}, \quad dM_t(x)=\rho(t,x)dx \tag{2.20}$$

are the microscopic and the macroscopic mass, respectively. The parameter $\theta\in[0,1]$ weights the coupling between the two scales, from $\theta=0$ corresponding to a purely macroscopic model to $\theta=1$ corresponding to a purely microscopic model. In (2.19) no scaling parameters explicitly appear, but we anticipate that

they will arise naturally from our next dimensional analysis. Using the measure (2.19), the mass conservation equation (2.2) takes the form of a mix of microscopic and macroscopic contributions

$$\begin{aligned}\frac{d}{dt}\left(\theta\sum_{j=1}^{N}\Phi(P_j(t)) + (1-\theta)\int_{\mathbb{R}^d}\rho(t,x)\Phi(x)dx\right) &= \theta\sum_{j=1}^{N}v(t,P_j(t))\cdot\nabla\Phi(P_j(t)) + \\ (1-\theta)\int_{\mathbb{R}^d}\rho(t,x)v(t,x)\cdot\nabla\Phi(x)dx, \quad \forall\Phi &\in C_c^\infty(\mathbb{R}^d), \end{aligned} \tag{2.21}$$

formally a convex linear combination of (2.11), (2.16). The interaction velocity $\nu[\mu_t]$ is now given by

$$\begin{aligned} v[\mu_t](P_j) &= \theta\sum_{\substack{k=1,\dots,N\\ P_k(t)\neq x}} f(|P_k(t)-x|)g(\alpha_{P_k(t)})\frac{P_k(t)-x}{|P_k(t)-x|} + \\ &\quad (1-\theta)\int_{\mathbb{R}^d} f(|y-x|)g(\alpha_{xy})\frac{y-x}{|y-x|}\rho(t,y)dy; \end{aligned} \tag{2.22}$$

therefore it coincides neither with the fully microscopic nor with the fully macroscopic one. This definitely makes the overall dynamics not a simple superposition of the individual microscopic and macroscopic dynamics. It is worth noticing that the point x may or may not be one of the positions of the microscopic pedestrians. Computing $\nu[\mu_t]$ for $x = P_j(t)$ shows that the interaction velocity of the j-th pedestrian does not only account for other microscopic pedestrians contained in the neighborhood of interaction but also for the macroscopic density distributed therein, which represents some crowd whose subjects are not individually modeled. Specifically, the term responsible for this is

$$\int_{\mathbb{R}^d} f(|y-P_j(t)|)g(\alpha_{P_j(t)y})\frac{y-P_j(t)}{|y-P_j(t)|}\rho(t,y)dy, \tag{2.23}$$

that we may regard as the macroscopic contribution to the microscopic dynamics. Analogously, computing $\nu[\mu_t]$ for x different from all of the P_j 's shows that the interaction velocity of an infinitesimal reference volume centered in x does not only depend on the density distributed in the neighborhood of interaction but also

on the microscopic pedestrians therein, which play the role of singularities in the average crowd distribution due to the granularity of the flow. The corresponding term is

$$\sum_{\substack{k=1,\dots,N \\ P_k(t)\neq x}} f(|P_k(t)-x|)g(\alpha_{P_k(t)y})\frac{P_k(t)-x}{|P_k(t)-x|} \tag{2.24}$$

which gives the microscopic contribution to the macroscopic dynamics.

2.2.4 Dimensional analysis

In order to scale correctly the microscopic and the macroscopic contributions, it is convenient to refer to the nondimensional form of the model. For this, let us preliminarily notice that the main quantities involved in the equations have the following dimensions:

- $[t]$ = time
- $[x]$ = length
- $[v_{des}] = [\nu]$ = length/time
- $[f]$ = length/(time pedestrians)
- $[\mu_t]$ = pedestrians
- $[\rho]$ = pedestrians/length^d,

where "pedestrians" is actually a dimensionless unit. Additionally, g and θ are dimensionless. Let L, V , ϱ be characteristic values of length, speed, and density (in particular, V may be the desired speed introduced in (2.4)) to be used to define the following nondimensional variables and functions:

$$\begin{aligned} x^* &= \frac{x}{L}, \quad t^* = \frac{V}{L}t, \quad \nu^*[\mu^*_{t^*}](x^*) = \frac{1}{V}\nu[\mu_{\frac{L}{V}t^*}](Lx^*), \\ f^*(s^*) &= \frac{1}{V}f(Ls^*), \quad \rho^*(t^*,x^*) = \frac{1}{\varrho}\rho\left(\frac{L}{V}t^*, Lx^*\right), \quad P^*_j(t^*) = \frac{1}{L}P_j\left(\frac{L}{V}\right) \end{aligned}$$

Notice that, due to the choice of V as characteristic speed, the dimensionless desired velocity v^*_{des} turns out to be a unit vector.

In more detail, the nondimensional mass measure $\mu^*_{t^*}$ is given by

$$\begin{aligned} d\mu^*_{t^*} &= d\mu_{\frac{L}{V}t^*}(Lx^*) \\ &= \theta \sum\nolimits_j d\delta_{LP^*_j(t^*)}(Lx^*) + (1-\theta)\varrho\rho^*(t^*,x^*)L^d dx^* \\ &= \theta \sum\nolimits_j d\delta_{P^*_j(t^*)}(x^*) + (1-\theta)\Lambda\rho^*(t^*,x^*)dx^* \\ &= \theta dm^*_{t^*}(x^*) + (1-\theta)\Lambda dM^*_{t^*}(x^*), \end{aligned}$$

where we have set $\Lambda := \varrho L^d$ and we have recognized the dimensionless microscopic and macroscopic masses

$$m^*_{t^*} = \sum_{j=1}^{N} \delta_{P^*_j(t^*)}, \qquad dM^*_{t^*}(x^*) = \rho^*(t^*, \cdot x^*)dx^*.$$

We notice that the coefficient Λ has unit $[\Lambda]$ = pedestrians; therefore it is a nondimensional number fixing the scaling between the microscopic and the macroscopic masses. It says how many pedestrians are represented, in average, by a unit density ρ^* in the infinitesimal reference volume dx^*.

Remark 2 *The measure*

$$\mu^*_{t^*} = \theta m^*_{t^*} + (1-\theta)\Lambda M^*_t \tag{2.25}$$

can be read as a linear interpolation between the microscopic and the macroscopic mass via the parameter θ, provided $m^*_{t^*} + (1-\theta)\Lambda M^*_{t^*}$ are, up to scaling, the same mass; i.e., $m^*_{t^*}(\mathbb{R}^d) = \Lambda M^*_{t^*}(\mathbb{R}^d)$. As we can see in [14], in the multiscale model the microscopic and macroscopic masses are individually conserved in time; hence this can be achieved by setting

$$\Lambda = \frac{m^*_0(\mathbb{R}^d)}{M^*_0(\mathbb{R}^d)} = \frac{N}{M^*_0(\mathbb{R}^d)}$$

as long as $0 < N$, $M^*_0(\mathbb{R}^d) < +\infty$. In the following we will invariably refer to the nondimensional form of the equations, mitting the asterisks on the nondimensional variables for brevity.

2.3 Discrete-in-time model

In this section we derive a discrete-in-time counterpart of the multiscale model, that will help us gain some insights into the qualitative properties of the mathematical structures previously outlined. In addition, it will serve as a first step to devise a numerical scheme for the approximate solution of the equations.

Let $\Delta t_n > 0$ be a possibly adaptive time step and let us introduce a sequence of discrete times $\{t_n\}_{n\geq 0}$ such that $t_0 = 0$ and $t_{n+1} - t_n = \Delta t_n$. Denoting $\mu_n := \mu_{t_n}$ from (2.3) with the choice $t_1 = t_n$, $t_2 = t_{n+1}$ we get

$$\begin{aligned}\int_{\mathbb{R}^d} \Phi(x) d\mu_{n+1}(x) - \int_{\mathbb{R}^d} \Phi(x) d\mu_n(x) &= \int_{t_n}^{t_{n+1}} \int_{\mathbb{R}^d} v(t,x) \cdot \nabla \Phi(x) d\mu_t(x) dt \\ &= \Delta t_n \int_{\mathbb{R}^d} v(t_n, x) \cdot \nabla \Phi(x) d\mu_n(x) + o(\Delta t_n),\end{aligned}$$

whence

$$\int_{\mathbb{R}^d} \Phi(x) d\mu_{n+1}(x) = \int_{\mathbb{R}^d} [\Phi(x) + \Delta t_n v(t_n, x) \cdot \nabla \Phi(x)] d\mu_n(x) + o(\Delta t_n).$$

At this point let us explicitly assume that $\mu_n(\mathbb{R}^d) < +\infty$. If $v(t_n, \cdot)$ is μ_n-uniformly bounded, then $\Phi(x) + \Delta t_n v(t_n, x) \cdot \nabla \Phi(x) = \Phi(x + \Delta t_n v(t_n, x)) + o(\Delta t_n)$; thus

$$\int_{\mathbb{R}^d} \Phi(x) d\mu_{n+1}(x) = \int_{\mathbb{R}^d} \Phi(x + \Delta t_n v(t_n, x)) d\mu_n(x) + o(\Delta t_n).$$

Defining the flow map $\gamma_n(x) := x + v(t_n, x)\Delta t_n$ and neglecting the term $o(\Delta t_n)$, we are finally left with

$$\int_{\mathbb{R}^d} \Phi(x) d\mu_{n+1}(x) = \int_{\mathbb{R}^d} \Phi(\gamma_n(x)) d\mu_n(x), \tag{2.26}$$

which makes sense actually for every bounded and Borel function Φ. Choosing $\Phi = \chi E$ for some measurable set $E \in \mathcal{B}(\mathbb{R}^d)$ entails

$$\mu_{n+1}(E) = \mu_n(\gamma_n^{-1}(E)), \quad \forall E \in \mathcal{B}(\mathbb{R}^d),$$

meaning that $\mu_n + 1$ is the push forward of μ_n via the flow map γ_n, also written $\mu_n + 1 = \gamma_n \# \mu_n$. Equation (2.26) provides a discrete-in-time counterpart of (2.3). Obviously, it requires to be supplemented by an initial condition μ_0 in order for the sequence $\{\mu_n\}_{n\geq 1}$ to be recursively generated.

Notice that, with the velocity field (2.4), it results $v(t_n, x) = v[\mu_n](x)$ with in particular

$$v[\mu_t](x) = \theta \sum_{\substack{k=1,\dots,N \\ P_k^n \neq x}} f(|P_k^n - x|) g(\alpha_{P_k^n}) \frac{P_k^n - x}{|P_k^n - x|} + \tag{2.27}$$

$$(1-\theta)\Lambda \int_{\mathbb{R}^d} f(|y-x|) g(\alpha_{xy}) \frac{y-x}{|y-x|} \rho_n(y) dy; \tag{2.28}$$

where $P_k^n := P_k(t_n)$ and $\rho_n(\cdot) := \rho(t_n, \cdot)$.

2.3.1 Preserving the multiscale structure of the measure

Recall that in the multiscale model we assumed that our measure is composed by a microscopic granular and a macroscopic continuous mass. Of course, this is just a formal assumption made to write the model. From the analytical point of view, it needs be proved that such a measure can be actually a solution to our equations.

Set $m_n := m_{t_n}$, $M_n := M_{t_n}$ so that, owing to (2.25), the measure μ_n can be given the form

$$\mu_{t^*}^* = \theta m_n + (1-\theta)\Lambda M_n \tag{2.29}$$

The result of Benedetti, Piccoli and Tosin [14] clarifies the role played by the flow map γ_n in preserving the multiscale structure of μ_n after one time step.

Chapter 3

Numerical approximation and Algorithms

3.1 Numerical approximation

Mantaining the measure-theoretic formalism all the problems of discretization of the density ρ can be bypassed. For the discretization in space of the density ρ_n we partition the domain in pairwise disjoint d-dimensional cells $E_i \in \mathcal{B}(\mathbb{R}^d)$, where $i \in \mathbb{Z}^d$ is an integer multi-index, sharing a characteristic size $h > 0$ such that $\mathcal{L}^d(Ei) \to 0$ for all i when $h \to 0^+$ (for instance, $h \sim \text{diam}E_i$). Every cell is further identified by one of its points x_i, e.g., its center in case of regular cells.

We approximate ρ by a piecewise constant function $\tilde{\rho}_n$ on the numerical grid

$$\tilde{\rho}_n(x) \equiv \rho_i^n, \quad \forall x \in E_i \tag{3.1}$$

where $\rho_i^n \geq 0$ is the value that $\tilde{\rho}_n$ takes in the cell E_i. Consequently, the measure M_n is approximated by the piecewise constant measure $d\tilde{M}_n = \tilde{\rho}_n d\mathcal{L}^d$, which entails the pproximation $\tilde{\mu}_n = \theta m_n + (1-\theta)\Lambda\tilde{M}_n$ for μ_n.

Analogously, we approximate the velocity $v[\mu_n]$ by a piecewise constant field

$$\tilde{v}[\tilde{\mu}_n] \equiv v_i^n, \quad \forall x \in E_i$$

where the values $v_i^n \in \mathbb{R}^d$ are computed as $v_i^n = v[\tilde{\mu}_n](x_i)$. The discretization of the velocity gives rise to the following discrete flow map:

$$\tilde{\gamma}_n(x) = x + \tilde{v}[\tilde{\mu}_n](x)\Delta t_n,$$

which turns out to be a piecewise translation because $\tilde{v}[\tilde{\mu}_n]$ is constant in each cell.

Finally, we look for a piecewise constant approximation $\tilde{M}_{n+1}$ of M_{n+1} by imposing the push forward of M_{n+1} via the flow map $\tilde{\gamma}_n$:

$$\tilde{M}_{n+1}(E) = \tilde{M}_n(\tilde{\gamma}_n^{-1}(E)), \quad \forall E \in \mathcal{B}(\mathbb{R}^d).$$

In particular, choosing $E = E_i$ yields

$$\rho_i^{n+1} = \frac{1}{\mathcal{L}^d(E_i)} \sum_{k\in\mathbb{Z}^d} \rho_k^n \mathcal{L}^d(E_i \cap \tilde{\gamma}_n(E_i)), \quad \forall i \in \mathbb{Z}^d \tag{3.2}$$

which provides a time-explicit scheme to compute the coefficients of the density $\tilde{\rho}_{n+1}$ from those of $\tilde{\rho}_n$. Notice in particular that $\tilde{\gamma}_n(E_k)$ is simply the set $E_k + v_k^n \Delta t$.

Notice that this scheme is positivity-preserving, in the sense that $\tilde{\rho}_n \geq 0$ implies $\tilde{\rho}_{n+1} \geq 0$ as well; hence, by induction, $\tilde{\rho}_0 \geq 0$ implies $\tilde{\rho}_n \geq 0$ for all $n > 0$. Such a basic property is not as straightforward in usual numerical schemes for hyperbolic conservation laws. Indeed, unless suitable corrections are implemented, the latter may develop oscillations leading to locally negative approximate solutions even when the exact solution is not expected to be so.

Furthermore, considering that $\tilde{\gamma}_n$ is a translation in each grid cell and using the invariance of the Lebesgue measure under rigid transformations, we deduce

$$\int_{\mathbb{R}^d} \tilde{\rho}_{n+1}(x)dx = \sum_{k\in\mathbb{Z}^d} \rho_k^n \sum_{i\in\mathbb{Z}^d} \mathcal{L}^d(\tilde{\gamma}_n^{-1}(E_i) \cap E_k) = \sum_{k\in\mathbb{Z}^d} \rho_k^n \mathcal{L}^d(E_k) = \int_{\mathbb{R}^d} \tilde{\rho}_n(x)dx;$$

thus the approximate macroscopic mass $\tilde{M}_n$ is conserved in time.

3.2 Simulation's algorithm

The algorithm combines a microscopic and a macroscopic part. The former handles the evolution of pedestrian positions, updating a vector which stores the values $P_j^n \in \mathbb{R}^d$. The latter manages instead the evolution of the density, and at

every time step it updates the values ρ_i^n at the grid cells. The two models evolve by means of the same velocity field $\tilde{v}[\tilde{\mu}_n]$, thus guaranteeing coherence of the final solution. The velocity field must be defined at pedestrian positions $\{P_j^n\}_{j=1}^N$ for the microscopic part and at the grid cells $\{E_i\}_{i\in I}$ for the macroscopic part.

Let us introduce the following superscripts:

- micro: quantities defined at pedestrian positions,
- macro: quantities defined at grid cells,
- micro-for-micro: microscopic quantities computed at pedestrian positions,
- micro-for-macro: microscopic quantities computed at grid cells,
- macro-for-micro: macroscopic quantities computed at pedestrian positions,
- macro-for-macro: macroscopic quantities computed at grid cells.

The algorithm consists of the following steps.

1. *Initialization.* We fix the number N of microscopic pedestrians that we want to model, we define their positions, and we compute the coefficients ρ_i^0 of the initial density according to a local average of the microscopic mass. More precisely, we set
$$\rho_i^0 = \frac{m_0(B_\xi(x_i))}{\Lambda \mathcal{L}^d(B_\xi(x_i))}, \qquad i \in I$$
where m_0 is the microscopic mass at the initial time and $(B_\xi(x_i))$ is the ball centered in the center of the grid cell E_i with radius $\xi > 0$. The latter is tuned depending on the positions of the microscopic pedestrians, in such a way that the relation $\Lambda = m_0(\mathbb{R}^d)/\tilde{M}_0(\mathbb{R}^d)$ be satisfactorily fulfilled in the numerical sense ($\tilde{M}_0$ being the approximate macroscopic mass at the initial time).

2. *Microscopic part.* At time $t = t_n$ we compute the sum at the right-hand side of (2.27) for $x = P_j^n$ obtaining
$$\tilde{\nu}^{micro-for-micro} := \tilde{\nu}[m_n](P_j^n).$$

The same computation performed for $x = x_i$ gives instead

$$\tilde{\nu}^{micro-for-macro} := \tilde{\nu}[m_n](x_i)$$

which will be shared with the macroscopic part of the code.

3. Macroscopic part. At the same time instant $t = t_n$ we numerically evaluate the integral at the right-hand side of (2.27) for $x = x_i$, using the approximate density $\tilde{\rho}_n$ in place of ρ_n. This way we obtain

$$\tilde{\nu}^{macro-for-macro} := \tilde{\nu}[\tilde{M}_n](x_i)$$

Next we compute the same integral for $x = P_j^n$, which yields

$$\tilde{\nu}^{macro-for-micro} := \tilde{\nu}[\tilde{M}_n](P_j^n)$$

This component of the velocity field will be shared with the microscopic part of the code. In particular, the integrals involved in $\tilde{\nu}^{macro-for-macro}$ and $\tilde{\nu}^{macro-for-micro}$ are numerically evaluated via a first order quadrature formula.

4. *Desired velocity.* If the velocity field v_{des} is given analytically, the computation of $v_{des}^{micro} := v_{des}(P_j^n)$ and of $v_{des}^{micro} := v_{des}(x_i)$ is immediate. If instead v_{des} is defined on the numerical grid only, for instance because it comes from the numerical solution of other equations [30], then v_{des}^{micro} is computed by interpolation. Since we are assuming that all macroscopic quantities are piecewise constant, we coherently choose a zeroth order interpolation.

5. *Overall velocity.* We assemble the previous pieces as

$$\begin{aligned} \tilde{v}^{micro} \quad &: \quad = \tilde{v}[\tilde{\mu}_n](P_j^n) \\ &= \quad v_{des}^{micro} + \theta\tilde{\nu}^{micro-for-micro} + (1-\theta)\Lambda\tilde{\nu}^{macro-for-micro}, \end{aligned}$$

and analogously

$$\begin{aligned} \tilde{v}^{macro} \quad &: \quad = \tilde{v}[\tilde{\mu}_n](x_i) \\ &= \quad v_{des}^{macro} + \theta\tilde{\nu}^{micro-for-micro} + (1-\theta)\Lambda\tilde{\nu}^{macro-for-macro}. \end{aligned}$$

6. *Computation of* Δt.We compute the largest time step Δt allowed by condition [14] for the macroscopic velocity field $\tilde{v}^{macro}$.

7. *Advancing in time.* We update pedestrian positions and density according to [14], (3.2) by means of $\tilde{v}^{micro}$ and $\tilde{v}^{macro}$, respectively.

3.3 Optimization's algorithms

We assume that pedestrians are in motion within a bounded area Ω with the aim to reach an exit identified by a portion of the boundary of Ω. Fixing some parameters as the initial density and the exit position, we want to determine the position of one or two obstacles inside the walking area, in order to find the obstacle configuration which minimizes the pedestrians average exit time. The exit flow is given by:

$$f(t) = \sum_{i=a}^{b} \rho_{iN}^{t} \left| U_1 \Delta t \right|,$$

where a and b are the exit extremes, N the number of grid cells in each direction and Δt the time step.

Fixed a time horizon $[0, T]$, the average exit flow and total flow can be calculated as follows:

$$\begin{aligned} \int_0^T f(t)tdt &= \sum_{i=0}^{T} f(i)(i), \\ \int_0^T f(t)dt &= \sum_{i=0}^{T} f(i). \end{aligned}$$

The average exit time is equal to:

$$T_{exit} = \frac{\int_0^T f(t)tdt}{\int_0^T f(t)dt}.$$

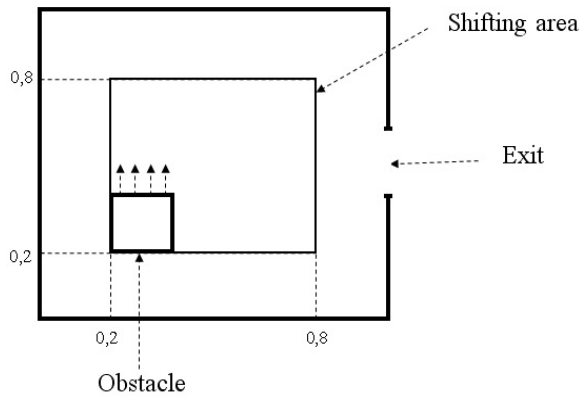

Figure 3.1: Configuration for the optimization

To find the optimal configuration with one obstacle we can apply two algorithms. The first one compares the average exit time obtained for all scenarios and consists of the following steps (see Figure 3.1):

(i) fix a shifting area of size $s < 1$ within the walking square;

(ii) assign the initial and final positions of the obstacle, given by the vertex left-down (for example $(0.2, 0.2)$ and $(0.6, 0.6)$, respectively);

(iii) choose the movement steps p $(0.1, 0.01$ or $0.001)$ for the obstacle;

(iv) move the left-down vertex of the obstacle in horizontal or vertical direction with step p from the initial position to the final one;

(v) the portion of the obstacle after each movement corresponds to a scenario x;

(vi) compute pedestrians average exit time for all obtained scenarios;

(vii) compare the average exit times for all scenarios.

The second algorithm is of steepest descent type according to which the obstacle configuration corresponding to the minimum exit time is found using the following iterative method:

(i) fix a shifting area of size $s < 1$ within the walking square;

(ii) assign randomly an initial position of the obstacle, through the coordinates of the left-down vetex (x_i, y_i), $i = 0$;

(iii) calculate the pedestrians average exit time $T(x_i, y_i)$ and partial derivates $\frac{\partial T(x_i,y_i)}{\partial x_i}$, $\frac{\partial T(x_i,y_i)}{\partial y_i}$;

(iv) compute the new position of the obstacle as follows:

$$(x_{i+1}, y_{i+1}) = (x_i, y_i) + h\left(\frac{\partial T(x_i, y_i)}{\partial x_i}, \frac{\partial T(x_i, y_i)}{\partial y_i}\right);$$

where h is the hessian matrix of $T(x_i, y_i)$ given by:

$$h = \begin{pmatrix} \frac{T_r+T_l-2T(x_i,y_i)}{\Delta x^2}, & \frac{(T_{ur}+T_{dl})-(T_{ul}+T_{dr})}{4\Delta x\Delta y} \\ \frac{(T_{ur}+T_{dl})-(T_{ul}+T_{dr})}{4\Delta x\Delta y}, & \frac{Tu+Td-2T(x_i,y_i)}{\Delta y^2} \end{pmatrix}; \tag{3.3}$$

where $T_r = T(x_i + 0.1, y_i)$, $T_l = T(x_i - 0.1, y_i)$, $T_d = T(x_i, y_i - 0.1)$, $T_{dl} = T(x_i - 0.1, y_i - 0.1)$, $T_{ul} = T(x_i - 0.1, y_i + 0.1)$, $T_u = T(x_i, y_i + 0.1)$, $T_{dr} = T(x_i + 0.1, y_i - 0.1)$ and $T_{ur} = T(x_i + 0.1, y_i + 0.1)$;

(v) if the point found is out of movement area, take the nearest point into movement area;

(vi) go to step (iii).

The minimum is reached when the new position is unchanged after a fixed number of runnings. A variant of this algorithm is obtained fixing h ($0.001, 0.003$ or 0.005).

The same algorithms can be used to perform optimization with two or more obstacles.

Chapter 4

Simulations and results

In this section we present the results of numerical simulations performed with the model and the algorithms described above. As natural for pedestrian flows, we deal with two-dimensional ($d = 2$) bounded domains, say $\Omega \subset \mathbb{R}^2$. This means that the mass possibly flowing out of the domain is considered as lost; i.e., it no longer affects the computation.

4.1 Optimization results

Let us find the optimal location of the obstacles, which minimize the average exit time for the following case study. Assume the initial density ρ_i^0, uniformly located in the position (x_i, y_i), $0,05 < x_i < 0,15$ and $0.1 < y_i < 0.9$; the exit point $(1, 0.5)$; the length of the obstacle side $l = 2$.

Fix movement step $p = 0.01$, with exhaustive exploration's algorithm we notice that:

(i) for a Dirichlet boundary condition, the obstacle's optimal position is $(0.2, 0.54)$ with average exit time: 147.92467 (Fig. 4.1);

(ii) for a Neumann boundary condition, the obstacle's optimal position is $(0.59, 0.2)$ with average exit time: 142.91435 (Fig. 4.2);

In each scenario, a compact group of pedestrians is initially positioned on the opposite side of the room and is guided toward the exit by either the field v_{des}, with the potential u set to zero at every internal and external boundary of Ω.

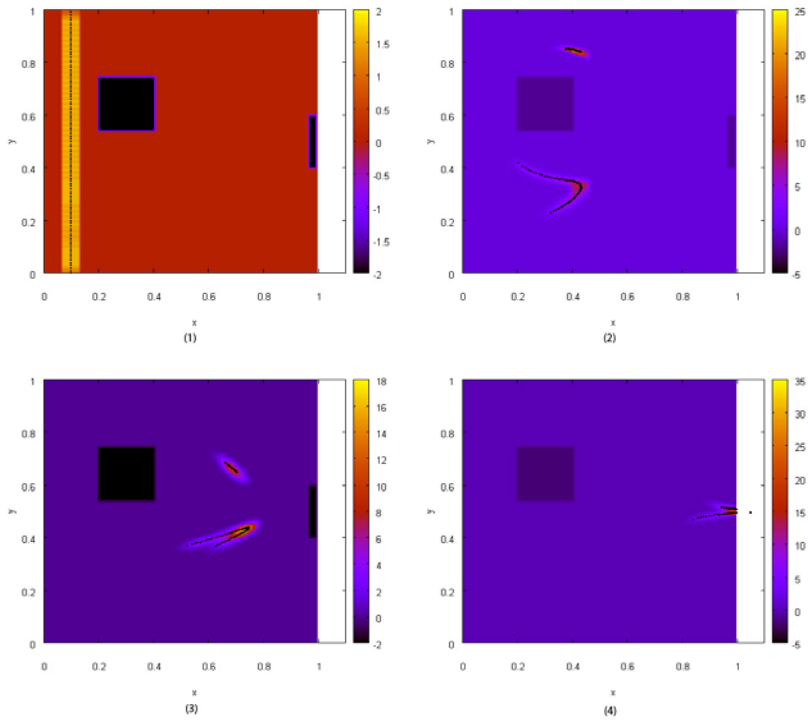

Figure 4.1: Optimal scenario with exhaustive exploration for Dirichlet boundary condition.

Starting from a compact cluster, the group expands and the density decreases. The repulsive effect of the obstacles is particularly evident in the case of Dirichlet boundary conditions, in fact the pedestrians passes relatively far from obstacle, while Neumann conditions produce instead the expected sliding of pedestrians along the edges. This demonstrates that the set of boundary conditions to generate the desired velocity field has in general nontrivial consequences on the resulting flow of pedestrians, and may vary from case to case also in connection with the role played by each obstacle in every specific application.

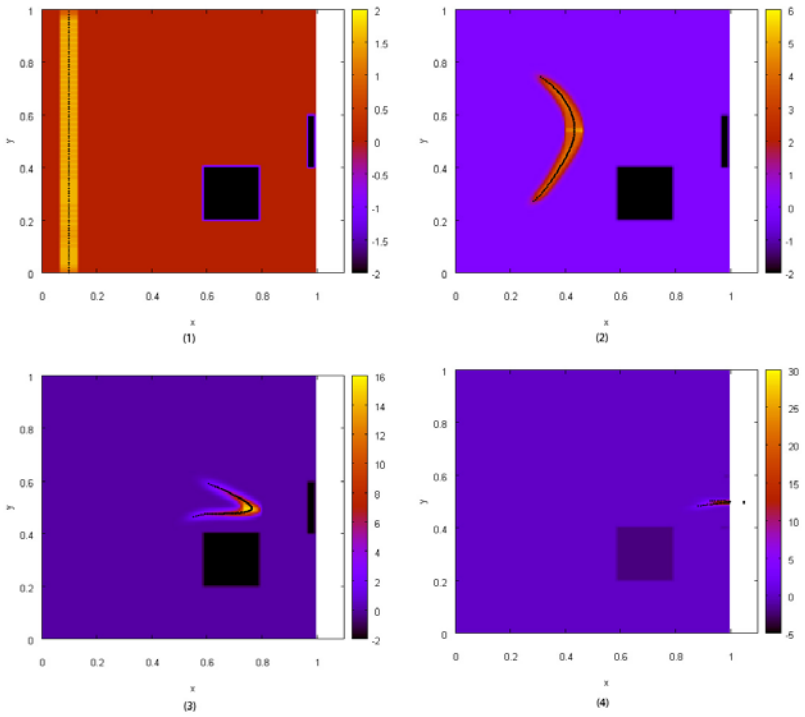

Figure 4.2: Optimal scenario with exhaustive exploration for Neumann boundary condition.

Start from the same initial configuration and apply the algorithm of steepest descent type fixing $h = 0.005$.

(i) for a Dirichlet boundary condition, with $x_0 = 0.4$, $y_0 = 0.5$ (see Figure 4.3) in 10 algorithm's steps we obtain a solution better than exhaustive exploration with step $p = 0.01$.The computed obstacle's optimal position is

$(0.20158692, 0.53415984)$ with average exit time: 147.91586;

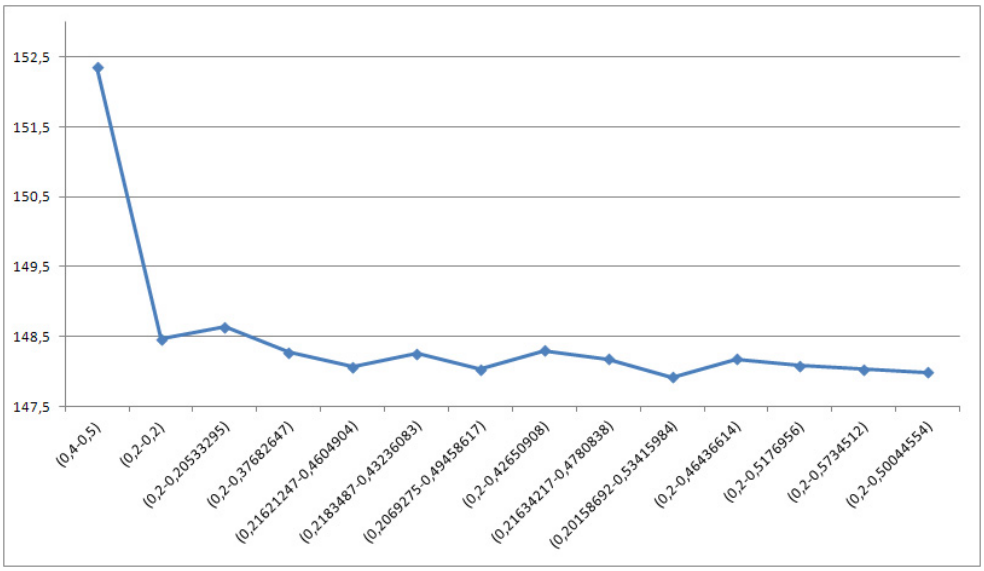

Figure 4.3: Steps of steepest descent type algorithm with Dirichlet boundary condition, $h = 0.005$ and $x_0 = 0.4$, $y_0 = 0.5$.

(ii) for a Neumann boundary condition, with $x_0 = 0.5$, $y_0 = 0.35$ (see Figure 4.4) in 13 algorithm's steps we obtain a solution better than exhaustive exploration with step $p = 0.01$.The obstacle's optimal position is $(0.5976594, 0.2)$ with average exit time: 142.8826.

Computing h as in (3.3) at every algorithm's step we obtain worst results, in fact:

(i) for a Dirichlet boundary condition, with $x_0 = 0.4$, $y_0 = 0.5$ (see Figure 4.5) in 3 algorithm's steps the obstacle's optimal position is $(0.39653486, 0.45202658)$ with average exit time: 149.76654;

(ii) for a Neumann boundary condition, with $x_0 = 0.4$, $y_0 = 0.6$ (see Figure 4.6) in 17 algorithm's steps the obstacle's optimal position is $(0.20741062, 0.57509136)$ with average exit time: 145.80989.

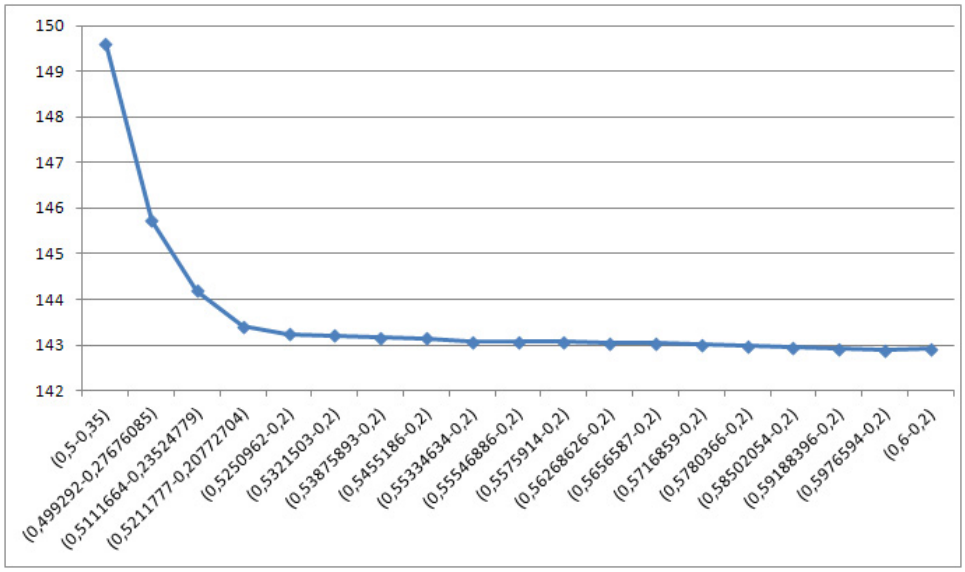

Figure 4.4: Steps of steepest descent type algorithm with Neumann boundary condition, $h = 0.005$ and $x_0 = 0.4$, $y_0 = 0.6$.

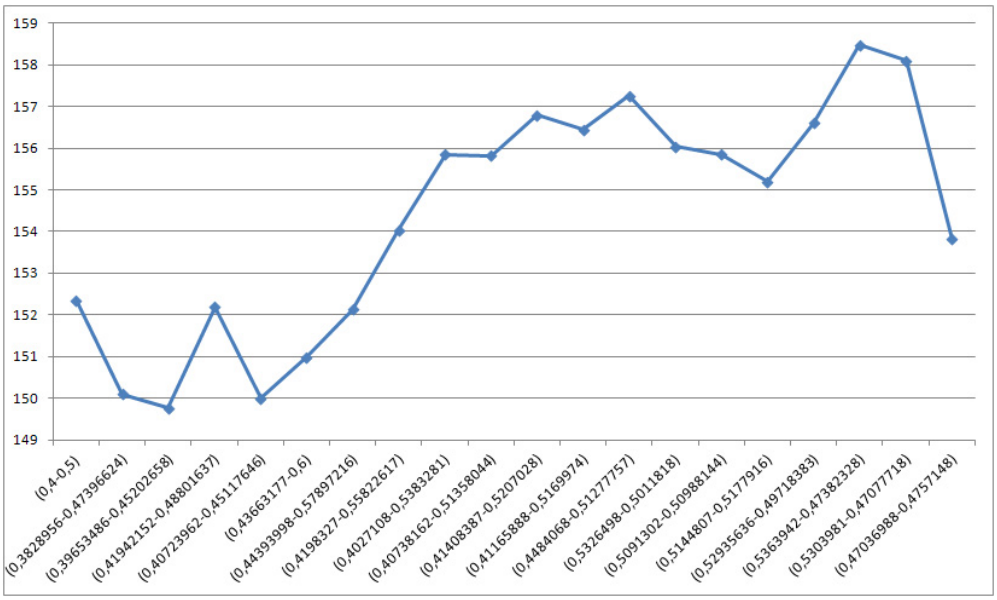

Figure 4.5: Steps of steepest descent type algorithm with Dirichlet boundary condition with $x_0 = 0.4$, $y_0 = 0.6$ and computing h as in (3.3) at every algorithm's step.

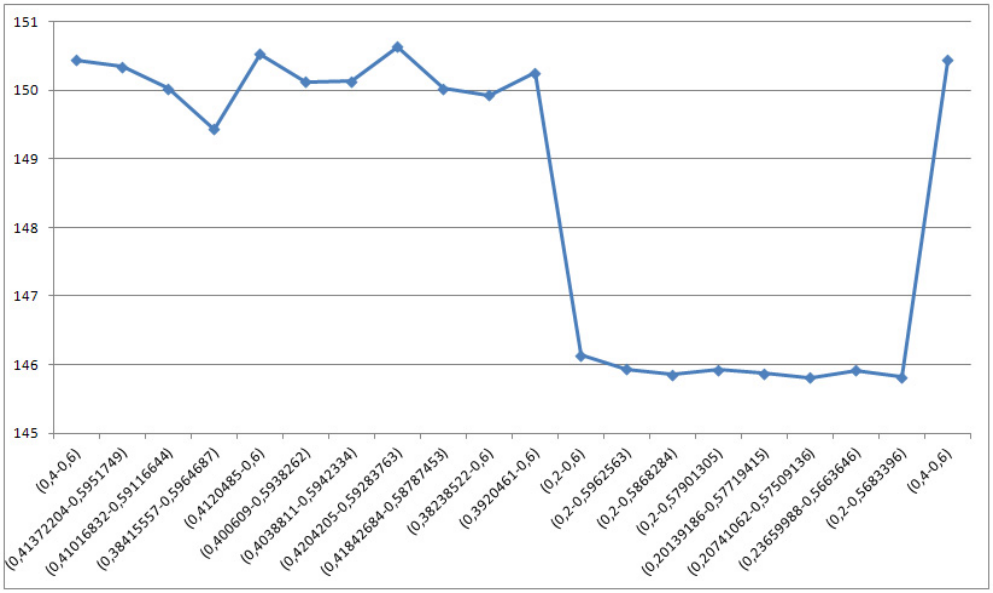

Figure 4.6: Steps of steepest descent type algorithm with Neumann boundary condition, $x_0 = 0.4$, $y_0 = 0.6$ and h given by (3.3) at every algorithm's step.

We can observe that fixing h we obtain a better result and the the algorithm converges linearly to a best solution while computing h as in (3.3) the algorithm fluctuates around best solution. Moreover, computing h at each step of the algorithm is very expensive.

4.2 Simulation of pedestrian dynamics in a flat

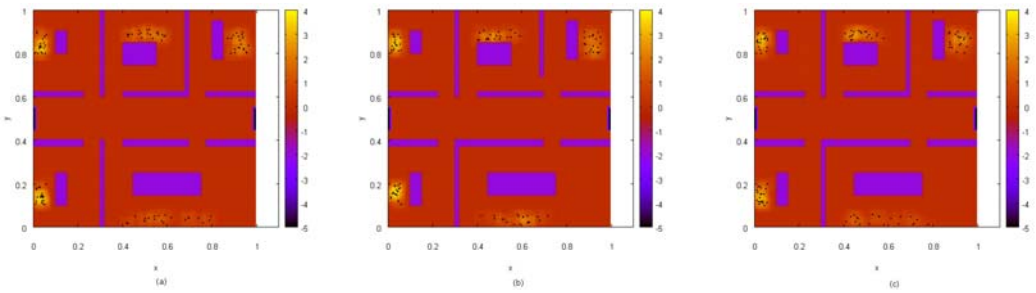

Figure 4.7: The flats scenarios.

In this section consider a bounded domain $\Omega \subset \mathbb{R}^2$ like a classical flat with five rooms, an obstacle inside, a corridor and two exits. In particular, for the computation of v_{des} we have set $u = 0$ on all outer boundaries of the walking area, so as to get a repulsive effect that leads pedestrians to walk away from perimeter walls and to occupy the middle of the corridor.

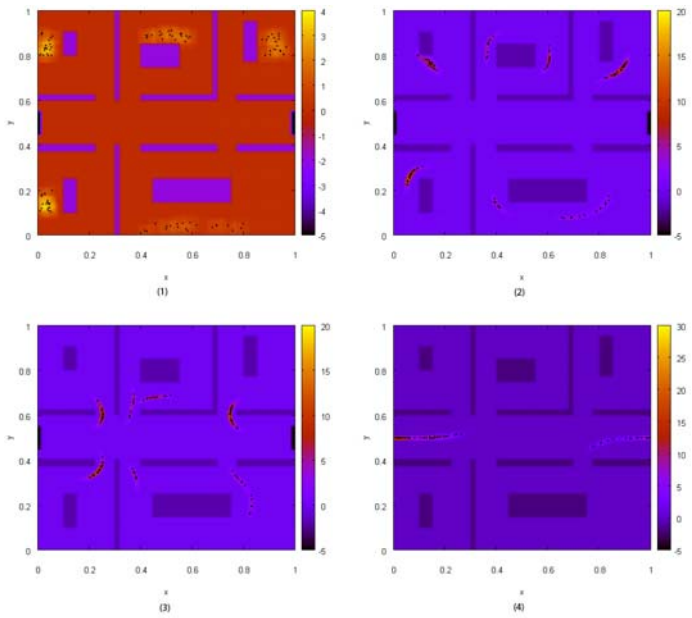

Figure 4.8: Optimal flat's scenario for Dirichlet boundary condition.

Fixing the exits and number of pedestrian $N = 100$ uniformly located in every room, changing the room's doors consider three different scenario (Figure 4.7) and compute the average exit time.

Using Dirichlet boundary condition we obtain the following average exit time for all scenarios: (a) 104.8413, (b) 105.40728, (c) 108.75423 (see Figure 4.8).

In Figure 4.8(1) we report the initial condition, i.e. the positions of all pedestrian inside the rooms. Some instant later, we notice that pedestrians pass relatively far from obstacles and walls (Figure 4.8(2)). Then, the pedestrians leave the rooms (Figure 4.8(3)) and seven little groups join in two big groups inside corridor that are directed toward exit (Figure 4.8(4)).

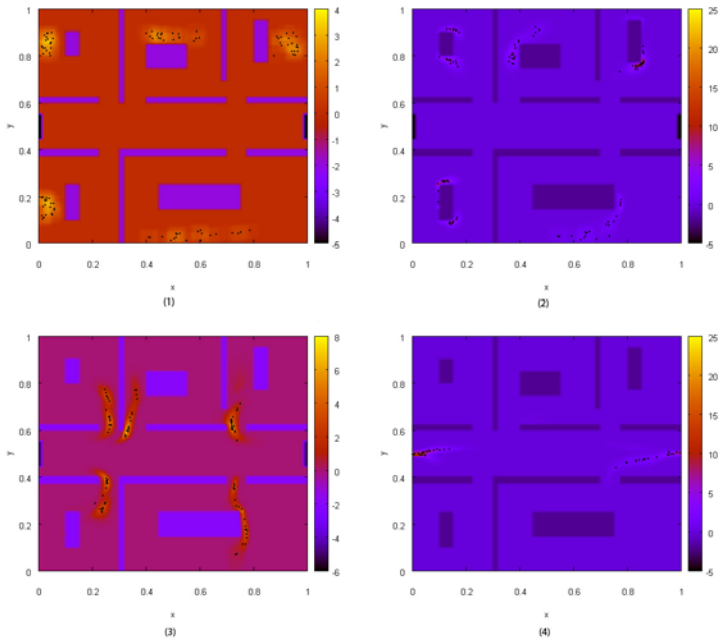

Figure 4.9: Optimal flat's scenario for Neumann boundary condition.

With Neumann boundary condition, the average exit time for all scenarios are follows: (a) 117.66598, (b) 109.76581, (c) 109.788 (see Figure 4.9).

The initial positions of all pedestrian inside the rooms with Neumann boundary condition are shown in Figure 4.9(1). The pedestrians pass near obstacles and walls (Figure 4.9(2)) because this boundary condition produce instead the expected sliding of pedestrians along the edges. Subsequently, the pedestrians leave the

rooms (Figure 4.9(3)) and the pedestrian join in two big groups inside corridor that are directed toward exit (Figure 4.9(4)).

Bibliography

[1] A. Aw and M. Rascle, *Resurrection of "second order" models of traffic flow*, SIAM J. Appl. Math., 60 (2000), 916–938.

[2] M. Ballerini, N. Cabibbo, R. Candelier, A. Cavagna, E. Cisbani, I. Giardina, V. Lecomte, A. Orlandi, G. Parisi, A. Procaccini, M. Viale, and V. Zdravkovic, *Interaction ruling animal collective behavior depends on topological rather than metric distance: Evidence from a field study*, Proc. Natl. Acad. Sci. USA, 105 (2008), pp. 1232–1237.

[3] C. Bardos, A. Y. le Roux, and J.-C. N ed elec. *First order quasilinear equations with boundary conditions.* Comm. Partial Differential Equations, 4(9):1017-1034, 1979.

[4] *Liverpool - History - Heysel disaster*, BBC Retrieved, 2011-03-22.

[5] *1989: Football fans crushed at Hillsborough*, BBC News, 15 April 1989 Retrieved 2 April 2010.

[6] N. Bellomo and C. Dogbé. *On the modelling crowd dynamics from scaling to hyperbolic macroscopic models*, Math. Models Methods Appl. Sci., 18(suppl.):1317-1345, 2008.

[7] H. Brezis, *Opérateurs Maximaux Monotones et Semi-groupes de contractions dans les espaces de Hilbert*, 1973.

[8] C. Canuto, F. Fagnani, and P. Tilli, *A Eulerian approach to the analysis of rendez-vous algorithms,* in Proceedings of the 17th IFAC World Congress, Seoul, Korea, 2008, pp. 9039–9044.

[9] P.G. Ciarlet, *Introduction à l'analyse numérique matricielle et l'optimisation*, Masson, Paris, 1990.

[10] R. M. Colombo and M. D. Rosini, *Existence of nonclassical solutions in a pedestrian flow model*, Nonlinear Anal. Real World Appl., 10, pp. 2716–2728, 2009.

[11] R. M. Colombo and M. D. Rosini. *Pedestrian flows and non-classical shocks*, Math. Methods Appl. Sci., 28(13):1553-1567, 2005.

[12] G. Colombo, M.D.P. Monteiro Marques, *Sweeping by a continuous proxregular set*, J. Differential Equations 187, no. 1, 46-62, 2003.

[13] V. Coscia and C. Canavesio, *First-order macroscopic modelling of human crowd dynamics*, Math. Models Methods Appl. Sci., 18 (2008), pp. 1217–1247.

[14] E. Cristiani , B. Piccoli, A. Tosin, *Multiscale modeling of granular flow with application to crowd dynamics*, Multiscale Model. Simul., 9(1):155-182, 2011.

[15] E. Cristiani, B. Piccoli, and A. Tosin, *Modeling self-organization in pedestrians and animal groups from macroscopic and microscopic viewpoints*, in Mathematical Modeling of Collective Behavior in Socio-Economic and Life Sciences, G. Naldi, L. Pareschi, and G. Toscani, eds., Birkh¨auser Boston, Cambridge, MA, 2010, pp. 337–364.

[16] E. Cristiani, P. Frasca, and B. Piccoli, *Effects of anisotropic interactions on the structure of animal groups*, J. Math. Biol., 2010, Online first (doi: 10.1007/s00285-010-0347-7).

[17] P. Dallard, T. Fitzpatrick, A. Flint, S. Le Btheirva, A. Low, R.M. Ridsdill, and M. Willford. *The London Millennium Footbridge,* The Structural Engineer, 79(22):17-33, 2001.

[18] J.F. Edmond, L. Thibault, *BV solutions of nonconvex sweeping process differential inclusion with perturbation*, J. Differential Equations 226, no. 1, 135-179, 2006.

[19] D. Helbing and A. Johansson, *Quantitative agent-based modeling of human interactions in space and time*, in Proceedings of The Fourth Conference of the European Social Simulation Association, 2007, pp. 623–637.

[20] D. Helbing and P. Molnar, *Social force model for pedestrian dynamics*, Phys. Rev. E, 51 (1995), pp. 4282–4286.

[21] D. Helbing, A. Johansson, and H. Z. Al-Abideen, *Dynamics of crowd disasters: An empirical study*, Phys. Rev. E, 75(4):046109, 2007.

[22] D. Helbing, T. Vicsek, *Optimal self-organization*, New J. Phys. 1, 13.1-13.17, 1999.

[23] D. Helbing, *Traffic and related self-driven many-particle systems*, Rev. Modern Phys., 73 (2001), pp. 1067–1141.

[24] R. L. Hughes, *A continuum theory for the flow of pedestrians*, Transportation Research Part B, 36:507-535, 2002.

[25] B. Maury and J. Venel, *Handling of contacts in crowd motion simulations*, in Traffic and Granular Flow '07, vol. 1, C. Appert-Rolland, F. Chevoir, P. Gondret, S. Lassarre, J.-P. Lebacque, and M. Schreckenberg, eds., Springer, Berlin, Heidelberg, 2007, pp. 171–180.

[26] B. Maury and J. Venel, *Un modèle de mouvements de foule*, ESAIM: Proceedings, 18:143-152, 2007.

[27] B. Maury and J. Venel, *A mathematical framework for a crowd motion model*, C. R. Math. Acad. Sci. Paris, 346 (2008), pp. 1245–1250.

[28] B. Maury, A. Roudneff-Chupin, and F. Santambrogio, *A macroscopic crowd motion model of gradient flow type*, Math. Models Methods Appl. Sci., 20 , pp. 1787–1821, 2010.

[29] J.J. Moreau, *Décomposition orthogonale d'un espace hilbertien selon deux cones mutuellement polaires*, C. R. Acad. Sci. 255, Série I, 238-240, 1962.

[30] B. Piccoli and A. Tosin, *Pedestrian flows in bounded domains with obstacles*, Contin. Mech. Thermodyn., 21 (2009), pp. 85–107.

[31] B. Piccoli, A. Tosin, *Time-evolving measures and macroscopic modeling of pedestrian flow*, Arch. Ration. Mech. Anal., 199(3):707-738, 2011

[32] F. Venuti and L. Bruno, *An interpretative model of the pedestrian fundamental relation*, C. R. Mecanique, 335 (2007), pp. 194–200.

[33] F. Venuti, L. Bruno and N. Bellomo, *Crowd dynamics on a moving platform: mathematical modelling and application to lively footbridges*, Math. Comput. Modelling, 45(3-4):252-269, 2007.